

THE REDSHIFT SEARCH RECEIVER 3 MM WAVELENGTH SPECTRA OF 10 GALAXIES

RONALD L. SNELL¹, GOPAL NARAYANAN¹, MIN S. YUN¹, MARK HEYER¹, AEREE CHUNG^{1,2}, WILLIAM M. IRVINE^{1,3}, NEAL R. ERICKSON¹, AND GUILIN LIU¹

Draft version October 25, 2018

ABSTRACT

The 3 mm wavelength spectra of 10 galaxies have been obtained at the Five College Radio Astronomy Observatory using a new, very broadband receiver and spectrometer, called the Redshift Search Receiver (RSR). The RSR has an instantaneous bandwidth of 37 GHz covering frequencies from 74 to 111 GHz, and has a spectral resolution of 31 MHz (~ 100 km s⁻¹). During tests of the RSR on the FCRAO 14 m telescope the complete 3 mm spectra of the central regions of NGC 253, Maffei 2, NGC1068, IC 342, M82, NGC 3079, NGC 3690, NGC 4258, Arp 220 and NGC 6240 were obtained. Within the wavelength band covered by the RSR, 20 spectral lines from 14 different atomic and molecular species were detected. Based on simultaneous fits to the spectrum of each galaxy, a number of key molecular line ratios are derived. A simple model which assumes the emission arises from an ensemble of Milky Way-like Giant Molecular Cloud cores can adequately fit the observed line ratios using molecular abundances based on Galactic molecular cloud cores. Variations seen in some line ratios, such as ¹³CO/HCN and HCO⁺/HCN, can be explained if the mean density of the molecular gas varies from galaxy to galaxy. However, NGC 3690, NGC 4258 and NGC 6240 show very large HCO⁺/HCN ratios and require significant abundance enhancement of HCO⁺ over HCN, possible due to the proximity to active galactic nucleus activity. Finally, the mass of dense molecular gas is estimated and we infer that 25-85% of the total molecular gas in the central regions of these galaxies must have densities greater than 10⁴ cm⁻³.

Subject headings: galaxies: ISM — ISM: Molecules — ISM: Abundances — Radio Lines: galaxies

1. INTRODUCTION

The molecular emission lines observed in galaxies are powerful probes of the physical and chemical properties of the gas most directly connected to the star formation process. Over the past several decades there have been many studies of the molecular line emission from galaxies, and these studies have provided invaluable information on the molecular gas content, star formation efficiency and molecular abundances (Young & Scoville 1991; Omont 2007). Although CO emission has been the primary means of deriving the molecular gas content in galaxies, emission from other less abundant molecular species, is much better in determining the physical and chemical properties of the gas. As the chemistry of the molecular gas is affected by the local radiation field, these trace molecular constituents may also provide information on local environments of this gas. More frequently observations of molecular species such as HCN, HCO⁺, HNC, and CS are being obtained (Omont 2007) and in a few cases mapped in nearby galaxies (Meier & Turner 2005). Since these molecules have much larger permanent electric dipole moments than CO, they require considerable higher densities to collisionally excite, and thus, in general, trace denser molecular gas than the gas probed by CO. Emissions from these dense gas tracers,

such as HCN, have been argued to be a much better probe of the star-forming molecular gas than emission from CO (Gao & Solomon 2004).

The utility of emission from these ‘high dipole moment molecules’ to probe the properties of the nuclear regions of galaxies is well established, and there have been numerous papers on this subject in recent years (see review by Omont (2007)). In addition, several emission line ratios, such as those for the low-lying transitions of HCN/CO, HCO⁺/HCN, and HNC/HCN, have been suggested as good diagnostics of the properties of the dense star-forming gas in galaxies (Aalto 2008). Nearly all studies of the molecular emission in galaxies have been limited to just a few targeted molecular lines. However, Martín et al. (2006) recently presented the first spectral scan of a galaxy providing an inventory of the molecular lines in NGC 253 within the 2 mm wavelength band. Such spectral scans can provide a much more complete description of the chemical complexities of the molecular gas in galaxies. The 3 mm wavelength band is equally well suited, and past spectral surveys have provided important information on the chemical and physical properties of Giant Molecular Clouds (GMCs) in the Milky Way (Johansson et al. 1984, 1985; Cummins et al. 1986; Turner 1989). One major disadvantage of most spectral line surveys is that the data are assembled from many observations with varying pointing accuracy and with potentially systematic calibration problems. The observations described here have been obtained *simultaneously* over the full spectral band for each galaxy, and hence many systematic problems are eliminated. In this paper we present the first 3 mm spectral scans of the central regions of 10 galaxies.

¹Department of Astronomy, LGRT 619, University of Massachusetts, 710 North Pleasant Street, Amherst, MA 01003; emails: snell@astro.umass.edu, gopal@astro.umass.edu, myun@astro.umass.edu, heyer@astro.umass.edu, irvine@astro.umass.edu, neal@astro.umass.edu, gliu@astro.umass.edu

²Harvard-Smithsonian Astrophysical Observatory, 60 Garden Street, Cambridge, MA, 02138; email: achung@cfa.harvard.edu

³Goddard Center for Astrobiology

2. OBSERVATIONS AND DATA REDUCTION

The observations reported in this paper were obtained in spring 2008 using the Redshift Search Receiver (RSR) on the Five College Radio Astronomy Observatory (FCRAO) 14-m telescope. The RSR is a sensitive, ultra-broad bandwidth receiver/spectrometer (Erickson et al. 2007) developed at the University of Massachusetts as a facility instrument for the 50-m diameter Large Millimeter Telescope (Schloerb 2008). This instrument was designed primarily to measure the redshift of distant, dust-obscured galaxies. The RSR is a dual polarization and dual beam instrument. The four broadband receivers cover instantaneously the frequency range 74-111 GHz. A high speed Faraday rotation beam switch, operating at 1 kilohertz, is used to overcome the $1/f$ noise originating in the front-end monolithic microwave integrated circuit (MMIC) amplifiers. Following the MMIC amplifiers, two wideband mixers convert each receiver band to two intermediate frequency (IF) channels. After further conversion and amplification, the IF signal is passed into an analog auto-correlation spectrometer. Each analog correlator has a bandwidth of 6.5 GHz and there are six correlators for each receiver polarization. To obtain the best frequency resolution, we do not apodize the lag domain signal before transforming to the frequency domain. Without this apodization, as with other auto-correlation based spectrometers, a ringing effect can be seen in the baselines around strong, narrow lines. The RSR has been designed to detect weak relatively broad lines, in which case this ringing is not a problem. In several of the spectra presented here, the ^{13}CO line is sufficiently strong, that this ringing adds additional baseline noise near the line. The RSR has an instantaneous bandwidth of 37 GHz with a resolution of 31 MHz, or a velocity resolution of approximately 100 km s^{-1} in the 3 mm wavelength band.

The RSR was commissioned on the FCRAO 14-m telescope in 2007 and 2008 and used for several initial science projects. During the time of the observations reported here, 12 of the final 24 spectrometers were available, which permitted beam switching with the full 37 GHz bandwidth in a single polarization. During commissioning observations, there was a small hardware issue (which has since been diagnosed and fixed) which produced anomalous noise at approximately 92 GHz, and a small region around this frequency has been blanked in many of the spectra presented here.

Observations were obtained at the positions of the 10 galaxies listed in Table 1. Distances in Table 1 for the nearby galaxies, NGC 253, Maffei 2, IC342 and M82, are from Karachentsev (2005) and distances for the more distant galaxies are from the NASA/IPAC Extragalactic Database. The galaxies were selected primarily because they were well studied and had relatively bright molecular emission lines, important for verifying the performance of the RSR. Since our observations cover the entire 3 mm wavelength window with uniform sensitivity, we can study the previously detected lines and all other lines within frequency range of the RSR. We added to the list of bright line galaxies some additional weak-line galaxies to further test the performance of the RSR and many of these additional galaxies are known to host an active galactic nucleus (AGN). Also included in the table

is the total integration time spent on each galaxy. The observations were taken over varying atmospheric conditions, so our broad aims were to achieve a relatively uniform sensitivity of about 1 mK or to achieve a signal to noise in the ^{13}CO line of 10. NGC 3079 and NGC 6240 did not show strong lines, so we spent additional time on these sources to lower the noise to better than 0.5 mK. The observations for each galaxy were obtained over several observing sessions and combined together. The pointing and calibration was repeatedly checked by observations of the continuum emission from planets and quasars. Pointing offsets were never more than a few arcseconds, a small fraction of the beam size, and the overall flux calibration is repeatable to be better than 10 %.

Also included in Table 1 are some brief notes regarding the properties of the central regions of the galaxies in our sample. The molecular emission in many of these galaxies is dominated by their nuclear starburst. Both NGC 6240 and Arp 220 are ultra luminous infrared galaxies (ULIRGS). NGC 1068, NGC 4258 and NGC 6240 all have Seyfert 2 nuclei; however, the emission we observe in NGC 1068 is likely dominated by the surrounding nuclear starburst ring (Schinnerer et al. 2000). NGC 4258 is a weak AGN, but has a pair of radio jets that may be influencing the molecular emission (Krause et al. 2007). NGC 6240 is the merger of two Seyfert 2 host galaxies where the two AGNs are separated by less than $2''$ and the molecular emission is concentrated in a small region centered on the Seyfert nuclei (Iono et al. 2007). Finally we note that NGC 3690 is in the process of merging with IC 694 (the system is called Arp 299 or Mrk 171). The nuclei of NGC 3690 and IC 694 are separated by only ~ 20 arcseconds and both nuclei have an AGN (García-Marín et al. 2006). The ^{13}CO and HCN emission from the IC 694 nucleus is much stronger than that from the NGC 3690 nucleus (Aalto et al. 1997); thus, although we are centered on NGC 3690, the emission may have a contribution from IC 694. Unfortunately, the emission from both nuclei is at approximately the same velocity, so velocity cannot be used to separate the emissions within our telescope beam.

One limitation of the RSR for the observations presented in this paper is the relatively small throw of the beam switch. The reference beam is only offset by 4.34 arcmin in azimuth. Thus, for the largest galaxies, such as IC 342 or NGC 253, the reference beam may contain weak emission from molecular clouds in the galactic disk. However, the ^{12}CO emission falls off sharply from the central regions, and even in the largest galaxies, the emission in the reference beam is more than 10 times weaker than that at the center of the galaxy (Young et al. 1995). As a check on line fluxes we compared the integrated intensity of the ^{13}CO emission, which of the lines we observe has the greatest potential for disk contamination, in the four galaxies (IC 342, NGC 253, NGC 1068 and NGC 3079) that were in common with the study of Paglione et al. (2001). Paglione et al. (2001) also used the FCRAO 14 m telescope; however they obtained their observations by position switching well off the galaxy. We find in all five galaxies that the integrated intensity we measure is in good agreement with that of Paglione et al. (2001); thus, we believe that the line integrated intensities that we report have not been strongly

affected by our beam switching observation mode.

The data have been analyzed using software developed by G. Narayanan specifically for RSR data reduction, and this software is a complete data reduction package with interactive graphics implemented using the Python programming language. For the data for each galaxy, linear baselines were subtracted from each of six spectral segments independently. The six segments were then combined together to form a spectrum covering 74 - 111 GHz. The complete spectrum of each of the 10 galaxies is presented in Figure 1. Note that due to the problems mentioned earlier, in many of the galaxies a small spectral window around 92 GHz has no usable data.

The RSR does not have Doppler tracking ability; thus, the spectra have a frequency axis in the local rest frame of the telescope. Due to changes in the Earth's motion relative to the sources, observations made at different times and on different days have slightly different frequency offsets, but these offsets are less than 5 MHz, much smaller than the 31 MHz resolution of the spectrometer. The intensity scales of all spectra shown are T_A^* (antenna temperature corrected only for atmospheric losses). The main beam efficiency of the 14-m telescope using the RSR has been measured to vary from 0.63 at 89 GHz to 0.51 at 107 GHz. The decline in efficiency at high frequencies is due to the increased amount of power lost to the error pattern of the telescope. The beam size also varied with frequency, with a HPBW of approximately 70" at 74 GHz decreasing to 47" at 111 GHz.

Since the galaxies observed vary enormously in distance, the regions probed by our RSR observations vary from spatial scales of approximately 1 kpc for the nearest galaxy to 18 kpc for the most distant galaxy. However, in many of these galaxies the molecular emission is centrally concentrated (Young et al. 1995), so that the observed emission is likely dominated by gas in the central ~ 1 Kpc region. It is worthwhile noting that the beam size variations over the RSR bandpass could distort line ratios if the emission were extended. However, if the bulk of the emission arises from a nearly unresolved source, then the line ratios will not be affected.

3. RESULTS

3.1. Line-integrated Intensities

The spectra shown in Figure 1 display a number of strong lines that are in common to almost all of the galaxies observed. In addition to the strong lines of ^{13}CO , HCN, HCO^+ , HNC and CS, many additional much weaker lines are also detected. The spectral scans of Orion KL and Sgr B2 (Turner 1989) were used as a guide to compile a list of spectral lines and line blends that are likely to be detectable in these galaxies and from this compilation we have identified all of the spectral features in the 10 galaxies. Lines from CO, CS, HCN, HCO^+ , HNC, N_2H^+ , C_2H , HNC, CH_3OH , HC_3N , C_3H_3 , SO and $\text{CH}_3\text{C}_2\text{H}$ are detected in one or more of these galaxies. In addition, at least one of the hydrogen recombination lines was detected in M82, NGC 1068 and NGC 4258.

One of the most important advantages of obtaining each 3 mm wavelength spectrum simultaneously with the RSR is the perfect pointing registration in all spectral lines. These galaxies all have complex small-scale struc-

ture, so even small pointing errors can seriously affect line ratios. In addition, because the lines were obtained simultaneously with a single instrument, the relative calibration of the spectral line intensities is very good.

The intensities of the spectral features were determined by fitting each spectrum with a template of spectral lines assuming a common line width and redshift. The list of lines was developed from the strong lines seen in the spectral scans of Orion and Sgr B2 (Turner 1989), and include all plausible lines, even if the chemistry is different than these Galactic sources. The benefit of such a simultaneous fit is that the line width and redshift can be well constrained by the stronger spectral lines, permitting more accurate determination of the intensities of the weaker lines. Of course this assumes that the emission from the various molecular species are distributed similarly so they share a common line width and line velocity. Examination of the residuals to the template fits finds them consistent with the baseline noise, thus, we believe that these assumptions are satisfied. The 33 spectral features that were fit are listed in Table 2, which include the isotopic lines of H^{13}CN , H^{13}CO^+ , HN^{13}C , and C^{34}S . Although these isotopic lines were not detected in any of the galaxies, they were included in the simultaneous fits to provide upper limits on the isotopic emission. Since hydrogen recombination lines were possibly detected in three of these galaxies, the entire series of hydrogen recombination lines were included in the fits. In several cases a single spectral feature was fit to a blend of lines (marked blend in Table 2) when the line separation in frequency was much smaller than the 31 MHz spectral resolution of the RSR. In most cases these were blends of lines from the same molecular species.

Fits to the 33 spectra features are shown superimposed on the spectra in Figure 1. All features with any significance are well fit by this line template. Features detected at a significance of 3σ or greater are labeled in Figure 1. The results of our template fitting procedure for all of the galaxies are summarized in Table 3. For features detected at a significance of 3σ or greater, the table provides the peak intensity and the 1σ uncertainty on these intensities (in parentheses). For features not detected at the 3σ significance level, the table provides the 3σ upper limit to the intensity of the spectral transition or blend. Only one of the six hydrogen recombination lines was detected in M82, however, two other recombination lines were just slightly below the detection threshold and remaining two recombination lines were present at the 2σ level. Thus, the presence of hydrogen recombination lines is probably secure. In NGC 1068 and NGC 4258 only the $\text{H}41\alpha$ recombination line was detected and in NGC 4258 this was only one of the three lines detected. In both of these galaxies there is no evidence for any of the other recombination lines at comparable strengths as the $\text{H}41\alpha$ line as would be expected, therefore, the identification of this feature at 92.035 GHz as a hydrogen recombination line is suspect. The only other plausible identification for this feature is a blend of CH_3CN lines from the $J = 5-4$ transition, however if correct, CH_3CN would be surprisingly strong in these two galaxies.

The only spectral line detected in all 10 galaxies is HCO^+ . ^{13}CO was detected in nine galaxies, HCN, HNC and CS were detected in seven galaxies and C^{18}O was detected in six galaxies. Because our sample of galaxies

vary in distance from 2.9 to 101 Mpc, the absolute detection threshold is not the same for these galaxies, however, in all subsequent analysis we utilize line ratios. The richest spectrum is that for NGC 253, where 16 of the 33 spectral features listed in Table 2 were detected. We note that there have been many spectroscopic observations of these same galaxies, and a number of the spectral lines in Table 2, not detected in our survey, were detected in more sensitive measurements focused on single spectral lines. In only six galaxies, Arp 220, NGC 1068, NGC 253, M82, IC 342, and Maffei 2, five or more spectral features are detected. In NGC 6240 the only line detectable is HCO^+ , and in two other galaxies, NGC 3690 and NGC 4258, we detect HCO^+ but not HCN. In the following section the template fits are used to examine several line intensity ratios and investigate variations in these ratios from galaxy to galaxy.

3.2. Measured Line Ratios

3.2.1. Isotopic Ratios

We first examine the CO isotopic ratios. In the six galaxies where both ^{13}CO and C^{18}O were detected, the average ratio $^{13}\text{CO}/\text{C}^{18}\text{O}$ was 4.5. The spread in this ratio was relatively small, ranging from 3.3 in NGC 3079 to 7.8 in Maffei 2. These measured ratios are similar to those found for massive GMCs in the disk of the Milky Way (Penzias et al. 1972) and for Sgr B2 (Cummins et al. 1986). A survey of luminous star-forming regions in the Milky Way (Loenen 2009) found $^{13}\text{CO}/\text{C}^{18}\text{O}$ ratios between 3 and 16, with the average region having a ratio of about 6, again very similar to the values measured in our galaxy sample. This ratio can be affected by optical depth; however, this lowest transition of CO is intrinsically weak, so it is expected that these isotopic lines are optically thin. Thus, this ratio likely reflects the abundance ratio of the isotopes of atomic carbon and oxygen. In the Milky Way both the $^{12}\text{C}/^{13}\text{C}$ ratio and the $^{16}\text{O}/^{18}\text{O}$ ratio have a strong dependence on galactic radius (Wilson 1999), both increasing with increasing galactic radius. Wilson & Rood (1994) suggest that both ^{13}C and ^{18}O are secondary nuclear products, while ^{12}C and ^{16}O are primary nuclear products. Ratios of primary to secondary products, such as $^{12}\text{C}/^{13}\text{C}$, are expected to be a good indicator of the chemical evolution of the Galaxy. However ratios of secondary products, such as $^{13}\text{CO}/\text{C}^{18}\text{O}$, should not vary greatly as is observed.

We did not detect the $J=1-0$ transitions of H^{13}CN , H^{13}CO^+ , or HN^{13}C or the $J=2-1$ transition of C^{34}S in any of the galaxies in our sample, however, these limits provide information on the optical depth of the main lines. The most sensitive limits on the isotopic line strengths were set in NGC 253 and M82. In NGC 253 the $3-\sigma$ lower limits on the isotopic intensity ratios were $\text{HCN}/\text{H}^{13}\text{CN} > 19$, $\text{HCO}^+/\text{H}^{13}\text{CO}^+ > 16$, and $\text{CS}/\text{C}^{34}\text{S} > 8$. In M82 the $3-\sigma$ lower limits were $\text{HCN}/\text{H}^{13}\text{CN} > 12$, $\text{HCO}^+/\text{H}^{13}\text{CO}^+ > 19$, and $\text{CS}/\text{C}^{34}\text{S} > 5$. If we assume isotopic abundances measured or NGC 253 summarized by Omont (2007), we conclude that the main isotopic lines of HCN, HCO^+ , HNC and CS have optical depths < 3 .

3.2.2. $\text{HCN}/^{13}\text{CO}$ Ratio

Both CO and HCN emission are often used as tracers of the molecular gas in galaxies (Omont 2007). Since the transitions of CO and HCN have quite disparate critical densities, they may be expected to trace different density molecular gas, and thus their ratio is a measure of the dense gas fraction (Paglione et al. 1998). ^{12}CO is outside the frequency range of the RSR for these very low redshift galaxies; however, we believe that ^{13}CO may be a much better probe of the gas. The ^{13}CO emission likely arises from higher column density molecular gas than CO, and much of the ^{13}CO emission may be produced in the same gas responsible for the HCN emission. Thus, the $\text{HCN}/^{13}\text{CO}$ ratio may be a good diagnostic of the density of the molecular gas most directly connected to the star formation activity in the nuclear starburst regions of these galaxies. We find that the $\text{HCN}/^{13}\text{CO}$ ratio varies significantly from galaxy to galaxy, with the largest ratio of 2.2 found in Arp 220 and the smallest ratio found in NGC 4258, where the $3-\sigma$ upper limit was only 0.30. We discuss later how this ratio can provide an important constraint on the mean gas density.

3.2.3. HCO^+/HCN Ratio

Early models of the chemistry of X-ray irradiated gas suggested that HCO^+ would be under-abundant in gas near a hard X-ray source (Lepp & Dalgarno 1996; Maloney et al. 1996). These results led to the suggestion that the HCO^+/HCN ratio may distinguish between PDR and XDR dominated gas and thus between central regions of galaxies dominated by either starbursts or AGNs. Subsequent observations (Kohno et al. 2001; Graciá-Carpio et al. 2006; Imanishi et al. 2007; Baan et al. 2008) seemed to confirm this prediction. These observations also showed an anti-correlation between the observed HCN/CO ratio and the HCO^+/HCN ratio. However, the more recent theoretical work of Meijerink & Spaans (2005) and Meijerink et al. (2007) places this interpretation in question. Meijerink et al. (2007) showed that in the high density gas, the HCO^+/HCN ratio is larger in XDR regions than in PDR regions, just the opposite of that suggested by Lepp & Dalgarno (1996). They also noted a strong density dependence for this ratio in both PDR and XDR gas.

In Figure 2 we plot the HCO^+/HCN ratio versus the $\text{HCN}/^{13}\text{CO}$ ratio. We find a similar trend to that found in previous observational papers, that is, the HCO^+/HCN ratio is inversely correlated with the $\text{HCN}/^{13}\text{CO}$ ratio. The agreement of our result with past papers is not surprising, since there is considerable overlap between our galaxy sample and those in the previous studies. We will address the role density plays in these ratio trends later, however, NGC 3690, NGC 4258 and NGC 6240 are quite anomalous in having unusually large ratios of HCO^+/HCN , and variations in chemistry are almost certainly needed to explain these ratios. NGC 6240 is not plotted in Figure 2 because we did not detect either HCN or ^{13}CO , but the ratio of HCO^+/HCN is greater than 2.3 (3 sigma limit). NGC 3690 and NGC 6240 were both part of the Juneau et al. (2009) study of ULIRGS, and these galaxies were among those with the largest HCO^+/HCN ratio.

3.2.4. HNC/HCN Ratio

The HNC/HCN ratio is a tracer of gas temperature (Aalto 2008). It is well known that in cold clouds the column density ratio of HNC/HCN can be as large as 3 to 10 (Churchwell et al. 1984), while in warm GMCs, the column density ratio is less than 1, and can be as small as 0.015 (Goldsmith et al. 1981). The strong dependence of this ratio on temperature is a prediction of molecular cloud chemistry (Schilke et al. 1992). Since these lines are similarly excited and have similar A -coefficients, when they are optically thin the observed emission ratio is proportional to the column density ratio. For the galaxies in our sample with detections in both lines, the observed ratio of HNC/HCN is confined to a narrow range of values between 0.43 and 0.69, narrower than that the galaxies observed by Aalto et al. (2002). The ratios are consistent with the emission arising from warm molecular gas.

3.3. Comparison of M82 and NGC 253

The two galaxies with the strongest emission lines are M82 and NGC 253 which enable a comparison of emission from other molecular species, such as C_2H , N_2H^+ , HNC, CH_3OH , HC_3N , C_3H_2 , SO and CH_3C_2H , that had only a limited number of detections in our galaxy sample as a whole. In both of these galaxies the emissions observed are likely dominated by molecular clouds associated with their nuclear starbursts. However there are differences, Aladro et al. (2011) suggested that the starburst in M82 is more evolved and the chemistry is dominated by PDR regions, while the chemistry in the younger starburst, NGC 253, is dominated by shocks.

Notable differences between these two galaxies are the detection of HNC, CH_3OH , N_2H^+ and HC_3N in NGC 253 but not in M82, although these lines would have been readily detected if they had the same line strength relative to HCN as they have in NGC 253. Both HNC and CH_3OH are thought to have a shock origin, as these molecules are believed to form on grain surfaces (Tideswell et al. 2010) and then ejected from the grains by low velocity shocks (Martín et al. 2008). Thus, the presence of these lines in NGC 253 agrees with the idea that shocks are an important component to the chemistry in the nuclear regions of this galaxy. Omont (2007) also noted that SiO and CH_3CN , both thought to have a shock origin, are more abundant in NGC 253 than M82. We note that HNC and CH_3OH are even stronger relative to HCN in IC 342 and Maffei 2, both whose chemistry may also be dominated by shocks (Aladro et al. 2011). A similar conclusion concerning IC 342 was reached by Meier & Turner (2005). The largest CH_3OH /HCN ratio was measured in NGC 3079, and thus the chemistry in NGC 253, IC 342, Maffei 2 and NGC 3079 may all be strongly influenced by shocks. HC_3N was also detected in NGC 253 and not in M82. The only other galaxy where HC_3N was detected was Arp 220, where the ratio of HC_3N /HCN was about three times larger than in NGC 253. Based on the strong emission in Arp 220 (Aalto et al. 2002), Aalto et al. (2007) speculated that strong HC_3N emission might be indicative of young starbursts and this perhaps may explain the stronger emission in NGC 253 relative to the older starburst M82.

The other notable difference is the detection of CH_3C_2H in M82 but not in NGC 253, and the CH_3C_2H /HCN ratio measured in M82 is three times larger than the 3σ upper limit established in NGC 253. In fact, other hydrocarbon molecules, such as C_2H , C_3H_2 and CH_3C_2H , have strengths relative to HCN much larger in M82 than in NGC 253. The enhancement of these hydrocarbon molecules in M82 is discussed in Fuente et al (2005) and they suggested that photon-dominated chemistry was important for the production of hydrocarbons in the central region of M82. Thus the pattern of lines seen in M82 and NGC 253 supports the suggestion of Aladro et al. (2011) that the chemistry in NGC 253 is influenced by shocks, while the chemistry in M82 is more PDR dominated.

3.4. Starburst Versus AGNs

From our sample of galaxies, we can also examine the differences between the starburst and AGN galaxies. We have already noted that NGC 3690, NGC 4258 and NGC 6240, all with AGNs, have anomalously large HCO^+ /HCN ratio. We have formed composite spectra of a sample of starburst galaxies (NGC 253, Maffei 2, IC 342, M82 and Arp 220) and galaxies with AGNs (NGC 1068, NGC 3690, NGC 4258 and NGC 6240). The emission in each spectra was first normalized to the strength of the HCO^+ line (the only line seen in all the galaxies), then the frequency axis was adjusted by a factor of $1+z$, and finally the spectra were averaged using equal weights. Equal weighting was used so that no galaxy dominated the composite spectrum, although this meant that the weaker line galaxies added more noise than the strong line galaxies to the composite spectra. The composite spectra were fit using the same procedure described earlier for the individual galaxies and, as before, a 3σ cutoff was used to define line detections. Unfortunately, the AGN composite consisted primarily of weak-line galaxies, so fewer lines were detected in the composite spectrum relative to the starburst composite. The most interesting ratio is the HCO^+ /HCN ratio and in the starburst galaxies this ratio has a value of 0.71 ± 0.06 , while in the AGN galaxies, the ratio was 1.9 ± 0.3 , significantly larger. We can also compare the $HCN/^{13}CO$ ratio, which for the starbursts was 1.11 ± 0.07 and for the AGNs was 0.64 ± 0.09 . Ratios of HNC/HCN and CS/HCN were similar in the two samples.

In the AGN galaxies, NGC 1068 has the strongest lines. Earlier we noted that none of the observed line ratios distinguishes NGC 1068 from the sample of starburst galaxies. The emission observed in NGC 1068 may be dominated by the starburst ring and not gas closely associated with the Seyfert nucleus. Removing NGC 1068, we can form a new AGN composite spectrum from the remaining three AGN galaxies. Although HCN was not detected in any of the individual galaxies, it is readily detected in their composite spectrum. In this new composite AGN spectrum, we find ratios of HCO^+ /HCN = 3.4 ± 0.9 and $HCN/^{13}CO = 0.45\pm 0.12$. Not surprising, these ratios are even more extreme relative to the starburst sample than the AGN composite including NGC 1068.

4.1. Modeled Line Ratios

The line ratios discussed in the previous section depend on both the physical (density, column density, and temperature) and chemical (molecular abundance) properties of the gas. The information available in our spectra is inadequate to constrain all the needed gas properties. We have consequently modeled the line ratios with a very simplistic approach in which we assume that the emission arises from a collection of identical molecular cloud cores which are characterized by a single temperature and density, with equal abundances of the various molecular species. Molecular abundances were taken from the well studied Galactic GMC cores M17 and Ceph A summarized by Bergin et al. (1997). We further assume abundance ratios of $\text{CO}/\text{H}_2 = 1 \times 10^{-4}$ and $^{13}\text{CO}/\text{CO} = 2 \times 10^{-2}$; the resulting molecular abundances relative to H_2 are given in Table 4. An E/A ratio of 1 for CH_3OH and an ortho/para ratio of 3 for C_3H_2 were also assumed. The assumed molecular abundances are very similar to those derived by Martín et al. (2006) for NGC 253 based on their 2 mm wavelength spectral survey (see comparison in Table 4).

The emission from an ensemble of GMC cores was modeled with the RADEX code (Van der Tak et al. 2007) using the Einstein A -coefficients and collision rate coefficients from the Leiden Atomic and Molecular Database (Schöier et al. 2005). To compute the line intensities, besides the molecular abundances, the gas density, n , gas temperature, T , and the H_2 column density per unit line width, $N(\text{H}_2)/\Delta v$, need to be specified. Our standard GMC core model assumes $T = 35$ K, $n = 1 \times 10^5 \text{ cm}^{-3}$, and $N(\text{H}_2)/\Delta v = 1 \times 10^{22} \text{ cm}^{-2} (\text{km s}^{-1})^{-1}$. Line widths for GMCs in the Galactic disk are around 3 km s^{-1} (Snell et al. 1984), leading to a H_2 column density of $3 \times 10^{22} \text{ cm}^{-2}$. Molecular clouds near the center of our Galaxy, such as Sgr B2, have line widths around 20 km s^{-1} (Cummins et al. 1986), and for this line width the modeled H_2 column density is $2 \times 10^{23} \text{ cm}^{-2}$.

The line ratios computed from our standard model are compared with the observations of NGC 253, the galaxy with the richest spectrum, in Figure 3. Since HCN usually has the strongest emission of any of the 'high dipole moment' molecules, all intensity ratios are computed relative to HCN. Multiple lines were observed for several molecular species and for the line ratio analysis the 87.9252 GHz line for HNCO, the 96.7414 GHz line for CH_3OH and the 99.2999 GHz line for SO were used in forming the intensity ratios. For HC_3N , the two lines at 81.8815 and 100.0764 GHz, which were in the least line confused regions of the spectrum, were summed together. The line ratios for our standard core model agree well with those observed for NGC 253. The largest discrepancies between the observed and modeled line ratios is less than a factor of two. The observed ratios in this galaxy are well fit using this simple model.

Our model can also be used to address the sensitivity of the various line ratios to density and temperature. The line ratios were computed from the standard model for densities of 1×10^4 and $1 \times 10^6 \text{ cm}^{-3}$ and the resulting line ratios shown in Figure 3. For our assumed abundances, a density of $1 \times 10^5 \text{ cm}^{-3}$ is the better fit to the observed line ratios in NGC 253. Figure 3 illustrates that several of the line ratios, due to differences in the critical density

of the lines forming the ratio, are highly sensitive to density. As expected, one of the values most affected is the $\text{HCN}/^{13}\text{CO}$ ratio; however, in addition, the line ratios $\text{CH}_3\text{OH}/\text{HCN}$ and HNCO/HCN are also density sensitive. The temperature sensitivity of these ratios can also be explored, and in Figure 4 the observed line ratios in NGC 253 are compared to those derived from our standard model with density $1 \times 10^5 \text{ cm}^{-3}$ and with varying temperatures. Temperature has a much smaller effect on the line ratios than does density, largely because the molecular transitions we observed all arise from similar energy levels above the ground rotational state.

NGC 253 has been widely studied and there are a number of estimates of the density of the molecular gas. Based on fitting multiple lines of CS, HCN and HCO^+ led Martín et al. (2005) and Knudsen et al. (2007) to estimate a density of approximately $2 \times 10^5 \text{ cm}^{-3}$, higher than an earlier estimate based on H_2CO emission (Hüttemeister et al. 1997). Recently, Bayet et al. (2009) fit the CS emission from NGC 253 with a two-component model consisting of a cool, lower density component and a warm, higher density component. For the two velocity features in NGC 253, they found densities for the cooler component of order 2×10^4 and for the warmer component of order $2 \times 10^6 \text{ cm}^{-3}$. The density in our standard model agrees well with the single density fits of Martín et al. (2005) and Knudsen et al. (2007) and is consistent with the average of the components fit by Bayet et al. (2009). Based on this density, the abundances we assumed in our standard model, including those molecules (HNCO and CH_3OH) that may be produced in shocks, are consistent with the observations in NGC 253. A better determination of the physical properties of the molecular gas is needed to refine the abundance estimates.

Our model can be used to examine the anti-correlation between the HCO^+/HCN and $^{13}\text{CO}/\text{HCN}$ ratios shown in Figure 2. Overlaid on the data in Figure 2 is shown a line connecting the results for five models in which only the density is varied, from 1×10^4 to $1 \times 10^6 \text{ cm}^{-3}$. The comparison between data and models suggests that much of the variation observed in the $^{13}\text{CO}/\text{HCN}$ ratio can be explained if the average density of the molecular gas varies among these galaxies. For densities below $1 \times 10^4 \text{ cm}^{-3}$, it is difficult to produce detectable HCN or ^{13}CO emission without having unrealistically large column densities of these molecular species. Although the HCO^+/HCN ratio is not strongly affected by density, some of the anti-correlation found between this ratio and the $^{13}\text{CO}/\text{HCN}$ ratio can be explained by variations in the average density. Juneau et al. (2009) came to similar conclusion and the sensitivity of these line ratios to density is also apparent in the modeling presented by Meijerink et al. (2007). Based on the line ratios, and ignoring any chemical differences, the data suggest that the molecular gas in Arp 220 is the densest and the molecular gas in NGC 3079 the least dense. However, density alone cannot explain the large HCO^+/HCN line ratios measured in NGC 3690, NGC 4258 and NGC 6240, all with AGNs. In the models of Meijerink et al. (2007), only the XDR models predict HCO^+/HCN ratios greater than one, thus, if these XDR models are correct, it is possible that the AGN has an influence on the chemistry

and is responsible for the enhanced HCO^+ abundance in the central regions of these three galaxies. However, the large sample of ULIRGS presented by Juneau et al. (2009) show no correlation between the HCO^+/HCN ratio and whether these galaxies are believed to be AGN or star formation dominated, putting some doubt in this AGN hypothesis for the enhanced HCO^+ emission.

The comparison between models and observations can be extended to the line ratios measured for IC342, M82, Arp 220, Maffei 2, NGC 1068 and NGC 3079. These comparisons are shown in Figure 4. Since density has the greatest influence on the line ratios, only models with varying density at a fixed temperature of 35 K are included in this figure. Based on model comparisons shown in Figures 2 and 4, IC 342, Maffei 2 and NGC 3079 would be expected to have the lowest average gas density of $\sim 10^4 \text{ cm}^{-3}$. This low average density is borne out by the other density sensitive ratios. With this density, we find the abundances from our standard core model reproduce well the measured line ratios in these three galaxies. Similarly, the average density for M82 is expected to be somewhat larger ($\sim 3 \times 10^4 \text{ cm}^{-3}$) and assuming this density we confirm that the abundances of HC_3N , CH_3OH , N_2H^+ , and HNCO relative to HCN are smaller than in our standard model and for those found in NGC 253. Again based on the result shown in Figures 2 and 4, NGC 1068 is expected to have a somewhat larger average density ($\sim 10^5 \text{ cm}^{-3}$), while Arp 220 is expected to have the highest average density ($\sim 10^6 \text{ cm}^{-3}$). As suggested earlier, we find an overabundance of HC_3N relative to HCN in Arp 220 for any of the modeled densities. Thus if we allow for the average molecular gas density to vary from galaxy to galaxy, our standard model with fixed abundances provides a reasonable good fit to the measured ratios in these galaxies.

There have been a number of estimates of the average molecular gas density for galaxies in our sample. Most of these estimates utilize multiple transitions of a single molecular species, thus they are independent of derived abundances. However, despite this, estimates for a single galaxy can still differ by order of magnitude. Density estimates for IC 342 (Hüttemeister et al. 1997; Meijerink & Spaans 2005), Maffei 2 (Hüttemeister et al. 1997), M82 (Naylor et al. 2010), and Arp 220 (Greve et al. 2009) are in reasonable agreement with our estimates. The HCN line SEDS shown in Knudsen et al. (2007) are also consistent with the trend in density variations for the galaxies M82, NGC 253 and Arp 220. Fitting the gas in the central regions of these galaxies with a single density is an oversimplification and Bayet et al. (2009) and Aladro et al. (2011) have fit multiple-density components for NGC 253, M82, IC 342, Maffei 2 and NGC 1068. With the exception of M82, their column density weighted average density is consistent with our findings. For M82, both find a column density weighted density about an order of magnitude higher than that of Naylor et al. (2010).

4.2. Molecular Mass and Beam Filling Factor

The simple model we presented in the previous section, in which the molecular emission observed arises from an ensemble of identical cloud cores, can be used to estimate the beam filling factor and mass of molecular gas, independent of the X_{CO} -factor. Since the distances

of the galaxies in our sample vary enormously, the region probed ranges from just the central starburst core to nearly the entire galaxy. The linear diameter of the FCRAO beam at the frequency of the ^{13}CO line for the distance of these galaxies (D_B) is given in Table 5.

The beam surface area filling factor (f_{area}) is related to the observed antenna temperature of the line corrected for the main beam efficiency (T_{MB}), the line intensity from our model (T_{model}), the assumed core line width in the model (Δv_{model}), and the observed line width of the galaxy (Δv_{obs}), which is dominated by galactic rotation, by the following equation:

$$f_{\text{area}} = \frac{T_{MB}}{T_{\text{model}}} \frac{\Delta v_{\text{obs}}}{\Delta v_{\text{model}}}. \quad (1)$$

The observed ^{13}CO emission is used to estimate the beam filling factor from the above relation. The modeled intensity ratios, discussed previously, did not depend on the line width, however, the total integrated intensity, and hence the beam surface filling factor, does. We have no information on the line widths of cloud cores in these galaxies, so we assume a line width of 10 km s^{-1} for our model cores, which corresponds to an H_2 column density of $1 \times 10^{23} \text{ cm}^{-2}$. Although a density of $1 \times 10^5 \text{ cm}^{-3}$ was assumed, the emission from ^{13}CO has very little density dependence as long as $n \geq 1 \times 10^4 \text{ cm}^{-3}$. Based on the observed line intensities and line widths presented in Table 3, the computed beam area filling factor is summarized in Table 5. Not surprising, the beam filling factor is strongly dependent on galaxy distance. For the nearer galaxies, the beam area filling factor can be as large as 0.26, implying that one-fourth of the FCRAO $\sim 50''$ beam is covered with gas with a total gas column density of $1 \times 10^{23} \text{ cm}^{-2}$, corresponding to an A_v of approximately 100 mag. Similar beam area filling factors would have been found if we had used other molecular species, such as HCN or HCO^+ . However, the results would have been more sensitive to the assumed density of the cloud cores.

The molecular gas mass can also be estimated from our model. The mass is given by:

$$M = m_{\text{H}_2} N_{\text{model}} f_{\text{area}} d^2 \Omega_B, \quad (2)$$

where m_{H_2} is the mass of a molecular hydrogen molecule, N_{model} is the gas column density in the core model, d is the distance to the galaxy, and Ω_B is the main beam solid angle. As long as the ^{13}CO emission is optically thin, the mass determination is independent of many of the assumed core model parameters. However, two important parameters in deriving masses are (1) the assumed core gas temperature, as this affects the partition function, and (2) the assumed $^{13}\text{CO}/\text{H}_2$ ratio of 2×10^{-6} . The mass of molecular hydrogen derived from the above equation is summarized in Table 5. Because of the varying distance of these galaxies, the mass of the nearby galaxies (NGC 253, Maffei 2, IC 342 and M82) includes only the gas in the central 1 kpc regions, whereas for the most distant galaxies (NGC 3690 and Arp 220) it includes the entire molecular mass of the galaxy.

These mass estimates can be compared with those derived from CO using an assumed X_{CO} -factor. To make certain that we are comparing the mass from comparable regions of these galaxies, we have used CO observations

also obtained with the FCRAO 14-m telescope as part of the FCRAO Extragalactic CO Survey (Young et al. 1995). Observations of all of the galaxies except Maffei 2 are covered in this survey, and these observations were obtained with nearly an identical beam size as our observations of ^{13}CO . The CO fluxes from the survey are summarized in Table 5, where the integrated intensity to flux conversion factor provided in Young et al. (1995) was used.

To estimate the mass from the CO fluxes, an X_{CO} -factor of $1.8 \times 10^{20} \text{ cm}^{-2} (\text{K km s}^{-1})^{-1}$, was used which is representative of Galactic molecular clouds (Omont 2007). The molecular hydrogen gas mass can then be written (Kenney & Young 1989) as:

$$M(H_2) = 7.1 \times 10^3 d^2 S_{\text{CO}}, \quad (3)$$

where d is the distance in Mpc and S_{CO} is CO flux in units of Jy km s^{-1} . The masses derived from this expression are presented in Table 5. Mass estimates from CO are 1.2 - 4.3 times larger than that derived from ^{13}CO . It is possible to reconcile these masses if we either lower the ^{13}CO abundance, increase the gas temperature assumed in our core model, or decrease the X_{CO} -factor used. We cannot rule out any of these possibilities; however, a more likely scenario is that some of the CO emission is arising from lower density and lower column density gas that does not produce significant ^{13}CO emission. No matter what the reason for the mass difference, we can conclude that the mass of dense gas must represent a significant fraction of the total molecular gas in these galaxy centers.

We find that between about 25 and 85 % of the total molecular mass in these galaxies must have high density and column density. These properties are likely associated with the molecular clouds in the central ~ 1 kpc regions of these galaxies. Bally et al. (1987) estimated the mean density of the molecular gas in the inner 500 pc radius region of the Milky Way to be $2 \times 10^4 \text{ cm}^{-3}$, similar to the average density estimated for several of the galaxies in our survey. However, the properties of the molecular clouds in the disk of the Milky Way are quite different. Lee et al. (1990) mapped a 3 deg^2 region around $\ell = 24^\circ$ in both ^{13}CO and CS. Although, no estimate was made of the mean density of the gas, the quoted emission ratio of CS/ ^{13}CO of 0.008 is substantially lower than the range of ratios, 0.12 - 1.0, we measured for our galaxy sample. The largest CS/ ^{13}CO ratio was observed in Arp 220, which is also modeled to have the highest mean molecular gas density. Since this ratio is sensitive to the mean gas density, this comparison suggests that a large fraction of the molecular gas in the central regions of the galaxies in our sample, and the Milky Way, must be dense, while molecular clouds in the Milky Way disk have a much smaller fraction of dense gas. Studies of individual molecular clouds in the disk of the Milky Way (Carpenter et al. 1995) confirm this and show that high density and high column density cores represent only a small fraction of the area and mass of the molecular cloud.

5. SUMMARY

We have presented the 3 mm wavelength spectra of the central regions of ten relatively nearby galaxies. The spectra of each galaxy were obtained simultaneously with

the RSR. The important advantages of obtaining the 3 mm wavelength spectra simultaneously are the perfect pointing registration in all spectral lines and the very good relative calibration of the spectral line intensities. The only uncertainty in relative line intensities comes from the small variations of beam efficiency and beam size with frequency. Most of the lines that we detected arise from high-dipole moment molecules, which allows us to examine the physical and chemical properties of the dense gas in these galaxies. Although the galaxies in our survey are far from being a homogeneous sample, their differences can be exploited to study the extent to which various line ratios are found to vary and to what extent they require differences in the physical or chemical properties of the molecular gas.

The spectra were fit with a template with 33 spectral features to determine the line intensities. We detected 20 of the 33 spectral features in our template, and these features arose from 14 different atomic and molecular species. Based on the fitted line intensities, a number of line intensity ratios were examined. The $^{13}\text{CO}/\text{C}^{18}\text{O}$ and HNC/HCN line ratios are insensitive to density. The $^{13}\text{CO}/\text{C}^{18}\text{O}$ ratio was found to have a very narrow range of values, from 3.3 to 7.8, supporting the idea that both ^{13}C and ^{18}O are secondary nucleosynthesis products. The HNC/HCN ratio also was relatively constant from galaxy to galaxy, varying between 0.4 - 0.7 and consistent with the emission arising in relatively warm gas.

The emission from these galaxies was modeled with an ensemble of molecular cloud cores, each with a temperature of 35 K and a molecular hydrogen column density per unit line width of $1 \times 10^{22} \text{ cm}^{-2} (\text{km s}^{-1})^{-1}$. The molecular abundances were taken from well-studied Galactic clouds, although these abundances are consistent with those found in NGC 253 (Martín et al. 2006). The sensitivity of various line ratios to density and temperature was examined and it was found that density has the greatest affect. The HCN/ ^{13}CO ratio is particularly density sensitive, and we believe that the large variation observed for this ratio may be due to differences in the mean gas density in these galaxies. Varying the density from 10^4 to 10^6 cm^{-3} can explain the range of HCN/ ^{13}CO ratios observed and provide consistent results with the other density sensitive line intensity ratios. Varying the density can also help explain much of the observed variations in the HCO^+/HCN ratio. Thus, a simple model with fixed molecular abundances and varying density, fits well the 3 mm spectra of most of these galaxies. One of the most notable exceptions is the anomalously large HCO^+/HCN ratios detected in NGC 3690, NGC 4258 and NGC 6240, which cannot be fit without increasing the abundance of HCO^+ relative to HCN relative. Based on the XDR model of Meijerink et al. (2007), a plausible explanation is that the AGN activity in these galaxies is responsible altering the chemistry in these galaxies and producing the large HCO^+/HCN ratio.

The cloud core model was used to estimate the filling factor of dense, high column density gas in our beam and to estimate the mass of dense molecular gas. The derived beam filling factors are strongly correlated with distance, as our beam varies in linear size from about

0.8 Kpc in the nearest galaxies to over 17 Kpc in the most distant galaxies. In the nearby galaxies, beam filling factors as great as 0.26 are found, suggesting that the central regions of these galaxies have a high filling factor of dense, high column density gas. We compared our mass of dense gas with estimates based on CO and an assumed X_{CO} -factor and find that the dense gas represents approximately 25-85 % of the total molecular gas

in the central regions of these galaxies.

This work was supported by NSF grants AST 0096854, AST 0704966 and AST 0838222 and by NASA grant NNG04G155A. We thank Hugh Crowl and Bing Jiang who assisted in data collection and Lauren Harley who assisted in some of the data reduction and spectral line fitting.

REFERENCES

- Aalto, S., Radford, S. J. E., Scoville, N.Z. & Sargent, A. I. 1997, *ApJ*, 475, L107
- Aalto, S., Polatidis, A.G., Hüttemeister, S. & Curran, S.J., 2002, *A&A*, 381, 783
- Aalto, S., Monje, R. & Martín, S. 2007, *A&A*, 475, 479
- Aalto, S. 2008, *Ap&SS*, 313, 273
- Aladro, R., Martín-Pintado, J., Martín, S., Mauersberger, R. & Bayet, E. 2011, *A&A*, 525, 89
- Baan, W. A., Henkel, C., Loenen, A. F., Baudry, A. & Wiklind, T., 2008, *A&A*, 477, 747
- Bally, J., Stark, A., Wilson, W. & Henkel, C. 1987, *ApJS*, 65, 13
- Bergin, E. A., Ungerechts, H., Goldsmith, P.F., Snell, R.L., Irvine, W.M. & Schloerb, F.P., 1997, *ApJ*, 482, 267
- Bayet, E., Aladro, R., Martín, S., Viti, S., & Martín-Pintado, J. 2009, *ApJ*, 707, 126
- Carpenter, J.M., Snell, R.L. & Schloerb, F.P. 1995, *ApJ*, 445, 246
- Churchwell, E., Nash, A.G. & Walmsley, C. M., 1984, *ApJ*, 287, 681
- Cummins, S. E., Linke, R. A., & Thaddeus, P. 1986, *ApJS*, 60, 819
- Erickson, N., Narayanan, G., Goeller, R., & Grosslein, R. 2007, *ASP Conf. Ser. 375, From Z-Machines to ALMA: (Sub)millimeter Spectroscopy of Galaxies*, ed. A. J. Baker, J. Glenn, A. I. Harris, J.G. Mangum, M.S. Yun (San Francisco, CA: ASP), 71
- Fuente, A., García-Burillo, S., Gerin, M., Teyssier, D., Usero, A., Rizzo, J.R. & De Vicente, P. 2005 *ApJ*, 619, L155
- Gao, Y. & Solomon, P. M., 2004, *ApJ*, 606, 271
- Goldsmith, P.F., Langer, W.D., Ellder, J., Irvine, W. & Kollberg, E., 1981, *ApJ*, 249, 524
- Graciá-Carpio, J., García-Burillo, S., Planesas, P., & Colina, L., 2006 *ApJ*, 640, L135
- García-Marín, M., Colina, L., Arribas, S., Alonso-Herrero, A. & Mediavilla, E. 2006, *ApJ*, 650, 850
- Greve, T. R., Papadopoulos, P. P., Gao, R. & Radford, S. J. E. 2009, *ApJ*, 692, 1432
- Hüttemeister, S., Mauersberger, R. & Henkel, C. 1997, *A&A*, 326, 59
- Imanishi, M., Nakanishi, K., Tamura, Y., Oi, Nagisa, & Kohno, Kotaro, 2007, *AJ*, 134, 2366
- Iono, D., Wilson, C.D., Takakuwa, S., Yun, M. S., Petitpas, G.R., Peck, A. B., Ho, P.T.P., Matsushita, S., Pihlstrom, Y. M. & Wang, Z. 2007, *ApJ*, 659, 283
- Johansson, L. E. B., Andersson, C., Ellder, J., Friberg, P., Hjalmarson, A., Hoglund, B., Irvine, W. M., Olofsson, H. & Rydbeck, G. 1984, *A&A*, 130, 227
- Johansson, L. E. B., Andersson, C., Elder, J., Friberg, P., Hjalmarson, A., Hoglund, B., Olofsson, H., Rydbeck, G. & Irvine, W. M. 1985, *A&AS*, 60, 135
- Juneau, S., Narayanan, D. T., Moustakas, J., Shirley, Y. L., Bussman, R. S., Kennicutt, R. C., Vanden Bout, P. A. 2009, *ApJ*, 707, 1217
- Karachentsev, I. D. 2005, *ApJ*, 129, 178
- Kenney, J.D.P., Young, J.S. 1989, *ApJ*, 344, 171
- Kohno, K., Matsushita, S., Vila-Vilaró, B., Okumura, S. K., Shibatsuka, T., Okiura, M., Ishizuki, S., Kawabe, R., 2001, *ASP Conf. Ser. 249, The Central Kiloparsec of Starbursts and AGN: The La Palma Connection*, ed. J. H. Knapen, J. E. Beckman, I. Shlosman, & T. J. Mahoney (San Francisco, CA: ASP), 672
- Knudsen, K. K., Walter, F., Weiss, A., Bolatto, A., Riechers, D. A. & Menten, K. 2007, *ApJ*, 666, 156
- Krause, M, Fendt, C. & Neinger, N. 2007, *A&A*, 467, 1037
- Lee, Y., Snell, R. & Dickman, R. 1990, *ApJ*, 355, 536
- Lepp, S., & Dalgarno, A., 1996, *A&A*, 306, L21
- Loenen, E., 2009, Ph.D. thesis, Univ. of Groningen
- Maloney, R.R., Hollenbach, D.J. & Tielens, A.G.G.M. 1996, *ApJ*, 466, 561
- Martín, S., Martín-Pintado, J., Mauersberger, R., Henkel, C. & García-Burillo, S. 2005, *ApJ*, 620, 210
- Martín, S., Mauersberger, R., Martín-Pintado, J., Henkel, C., & García-Burillo, S. 2006, *ApJS*, 164, 450
- Martín, S., Requena-Torres, M.A., Martín-Pintado, J. & Mauersberger, R. 2008, *ApJ*, 678, 245
- Meier, D. S. & Turner, J. L. 2005, *ApJ*, 618, 259
- Meijerink, R. & Spaans, M., 2005, *A&A*, 436, 397
- Meijerink, R., Spaans, M. & Israel, F., 2007, *A&A*, 461, 793
- Naylor, B.J., Bradford, C.M., Aquirre, J.E., Bock, J.J., Earle, L., Glenn, J., Inami, H., Kamenetzky, J., Maloney, P.R., Matsuhara, H., Nguyen, H.T., & Zmuidzinas, J. 2010, *ApJ*, 722, 558
- Omant, A., 2007, *Rep. Prog. Phys.*, 70, 1099
- Paglionone, T., Jackson, J., Bolatto, A., & Heyer, M. 1998, *ApJ*, 493, 680
- Paglionone, T., Wall, W., Young, J., Heyer, M., Richard, M., Goldstein, M., Kaufman, Z., Nantais, J., & Perry, G. 2001, *ApJS*, 135, 183.
- Penzias, A. A., Jefferts, K. B., Wilson, R. W., Liszt, H. S., & Solomon, P. M., 1972, *ApJ*, 178, L35
- Schilke, P., Walmsley, C.M., Pineau Des Forets, G., Roueff, E., Flower, D.R. & Guilloteau, S., 1992, *A&A*, 256, 595
- Schinnerer, E., Eckart, A., Tacconi, L.J., Genzel, R. & Downes, D., 2000, *ApJ*, 533, 850
- Schloerb, F. P. 2008, *Proc. SPIE*, 7012
- Schöier, F.L., Van der Tak, F.F.S., van Dishoeck, E.F. & Blaauw, J. H., 2005, *A&A*, 432, 369
- Snell, R. L., Goldsmith, P. F., Erickson, N. R., Mundy, L. G. & Evans, N. J. II 1984, *ApJ*, 276, 625
- Tideswell, D.M., Fuller, G.A., Millar, T.J. & Markwick, A.J., 2010, *A&A*, 510, 85
- Turner, B. 1989, *ApJS*, 70, 539
- Van der Tak, F.F.S., Black, J.H., Schöier, F.L., Jansen, D.J. & van Dishoeck, E.F., 2007, *A&A*, 468, 627
- Wilson, T.L., 1999, *Rep. Prog. Phys.*, 62, 143
- Wilson, T.L. & Rood, R. 1994, *ARA&A*, 32, 191
- Young, J.S. & Scoville, N.Z. 1991, *ARA&A*, 29, 581
- Young, J.S. et al. 1995, *ApJS*, 98, 219

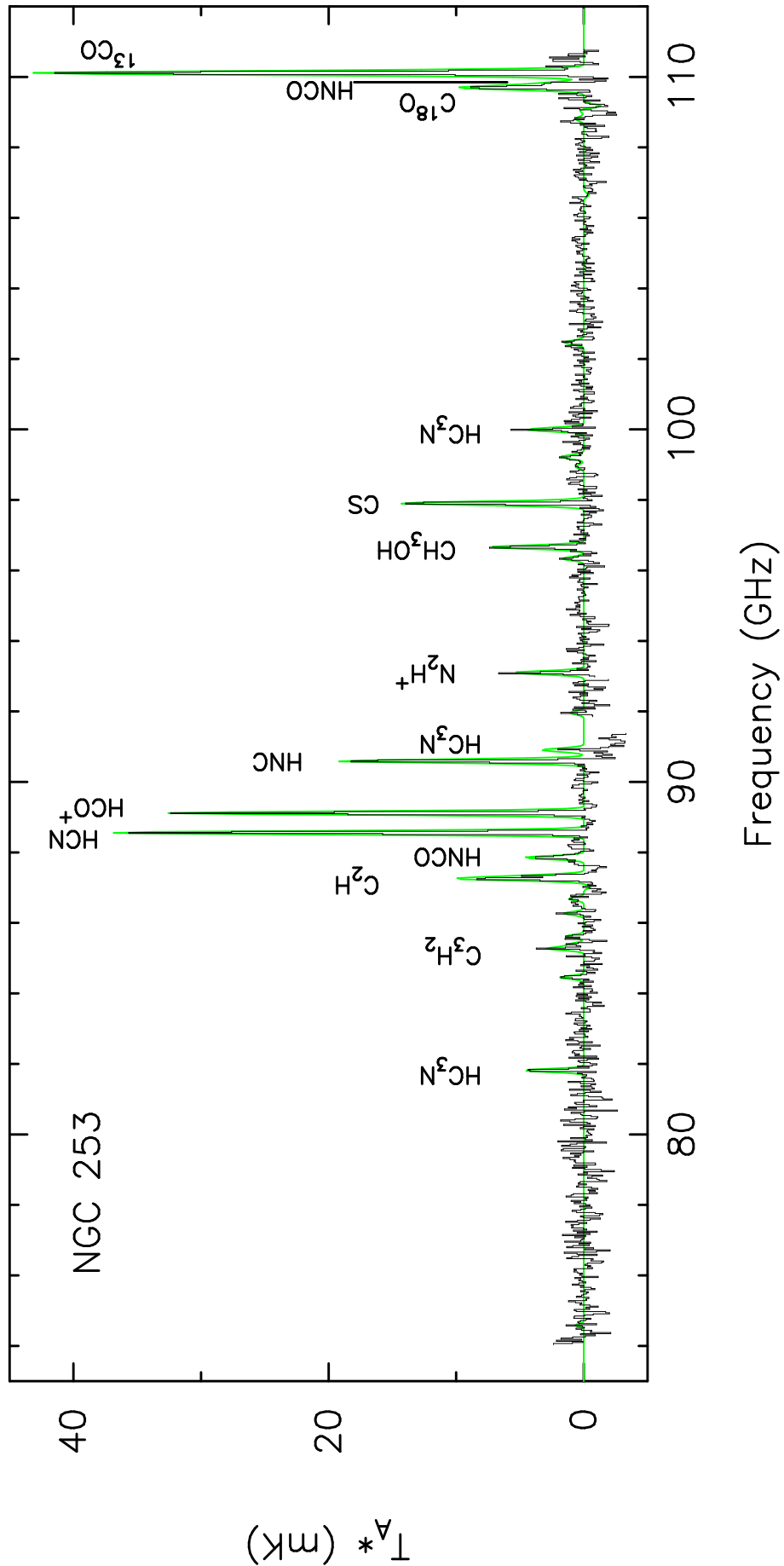


FIG. 1A.— Three-millimeter spectra for NGC 253 are presented by the binned points. The frequency axis is measured relative to the local rest frame of the telescope with no corrections for the Earth’s motion. The continuous line (continuous green line in the electronic version of the paper) shows the fit of our 33-spectral feature template discussed in the text.

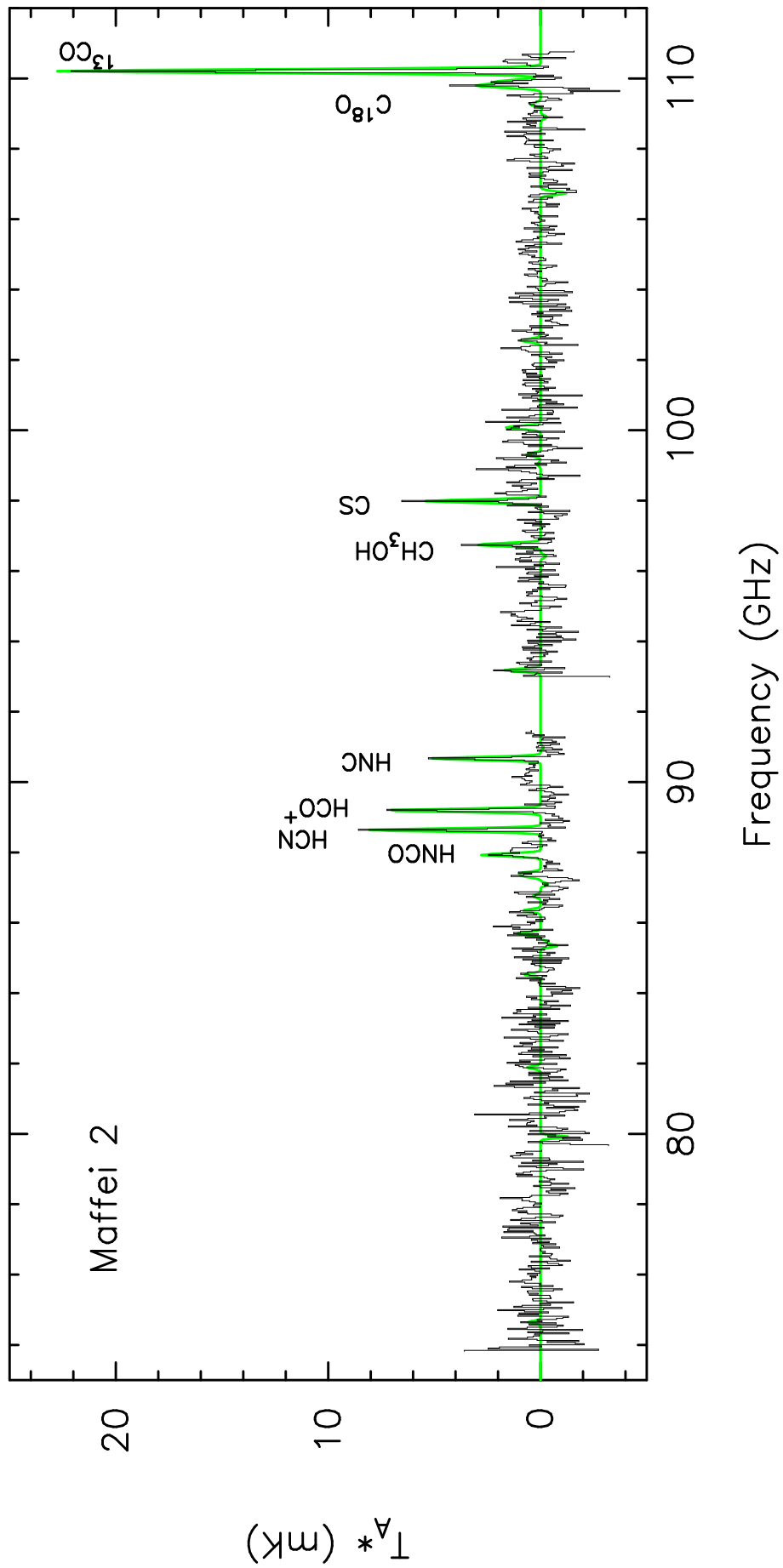


FIG. 1B.— Same as (a) for Maffei 2.

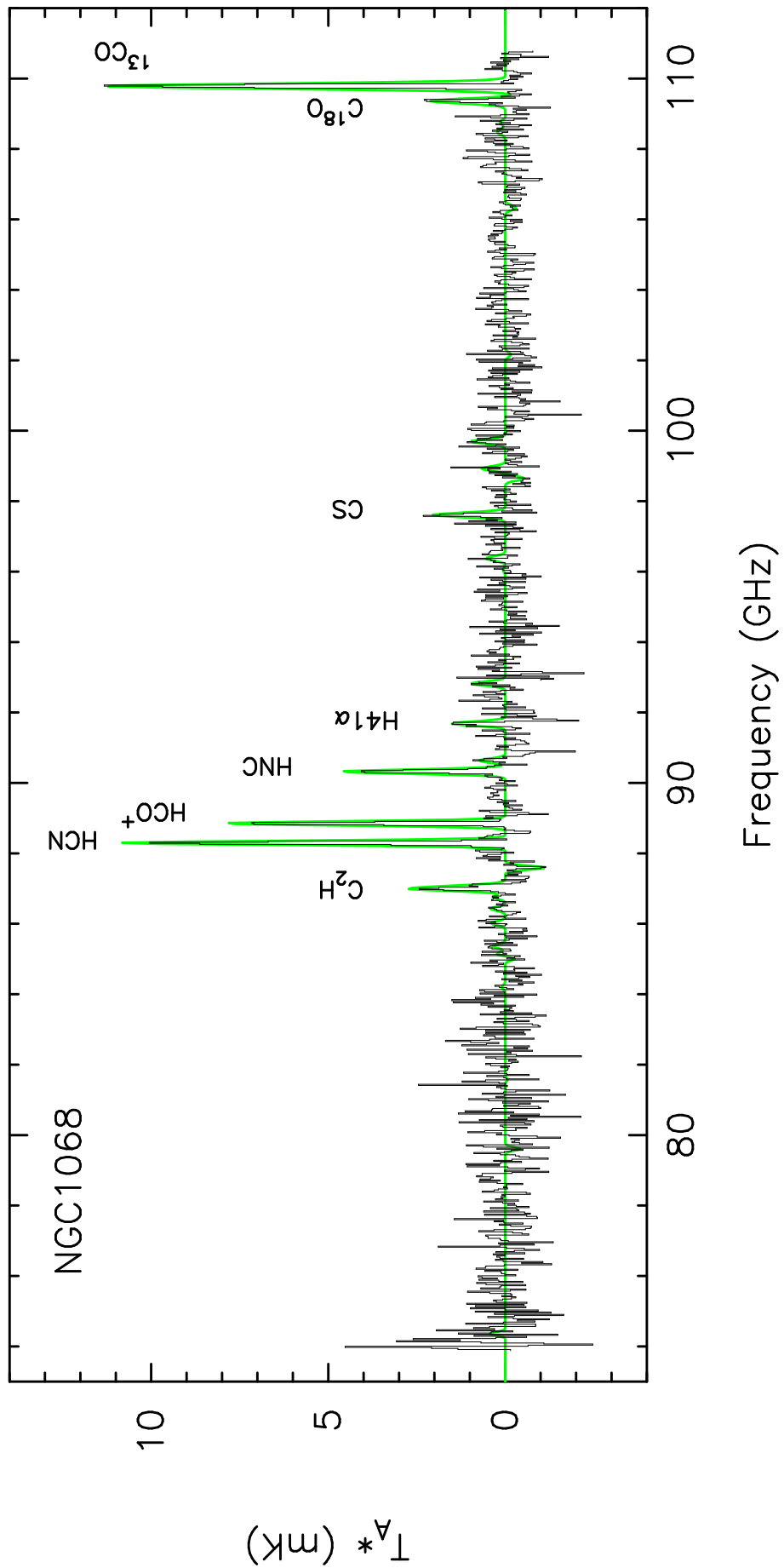


FIG. 1c.— Same as (a) for NGC 1068.

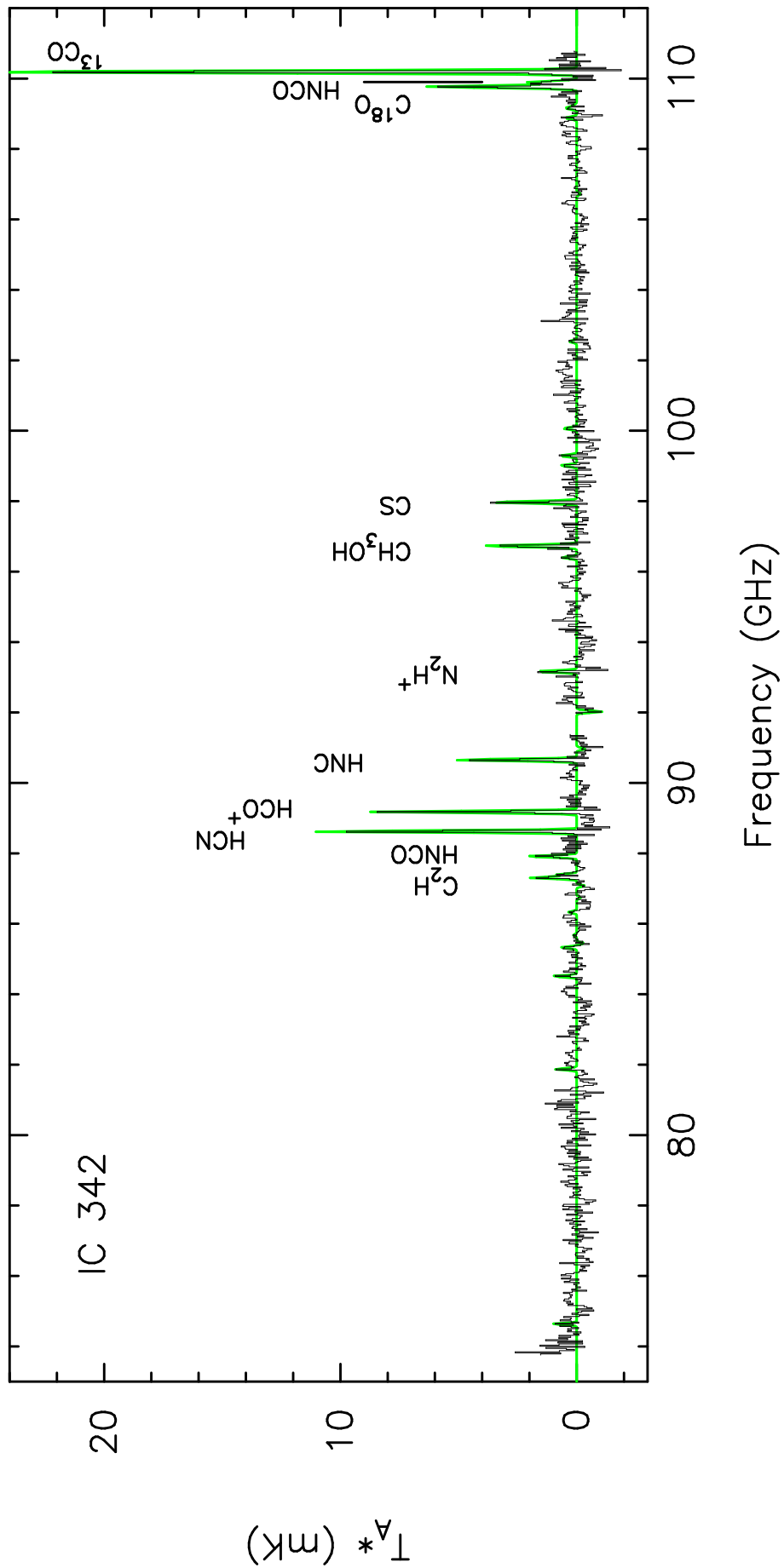


FIG. 1D.— Same as (a) for IC 342.

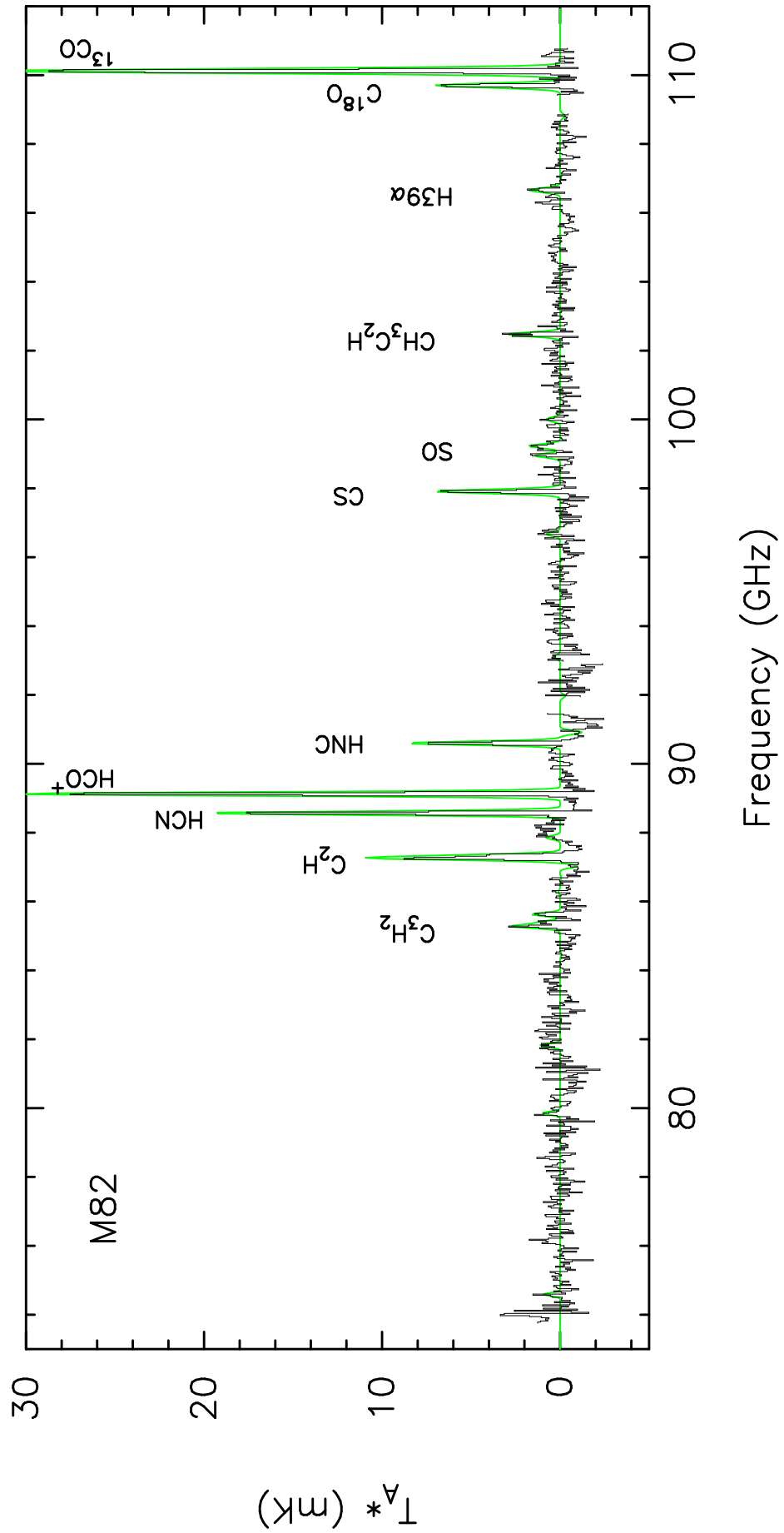


FIG. 1E.— Same as (a) for M82.

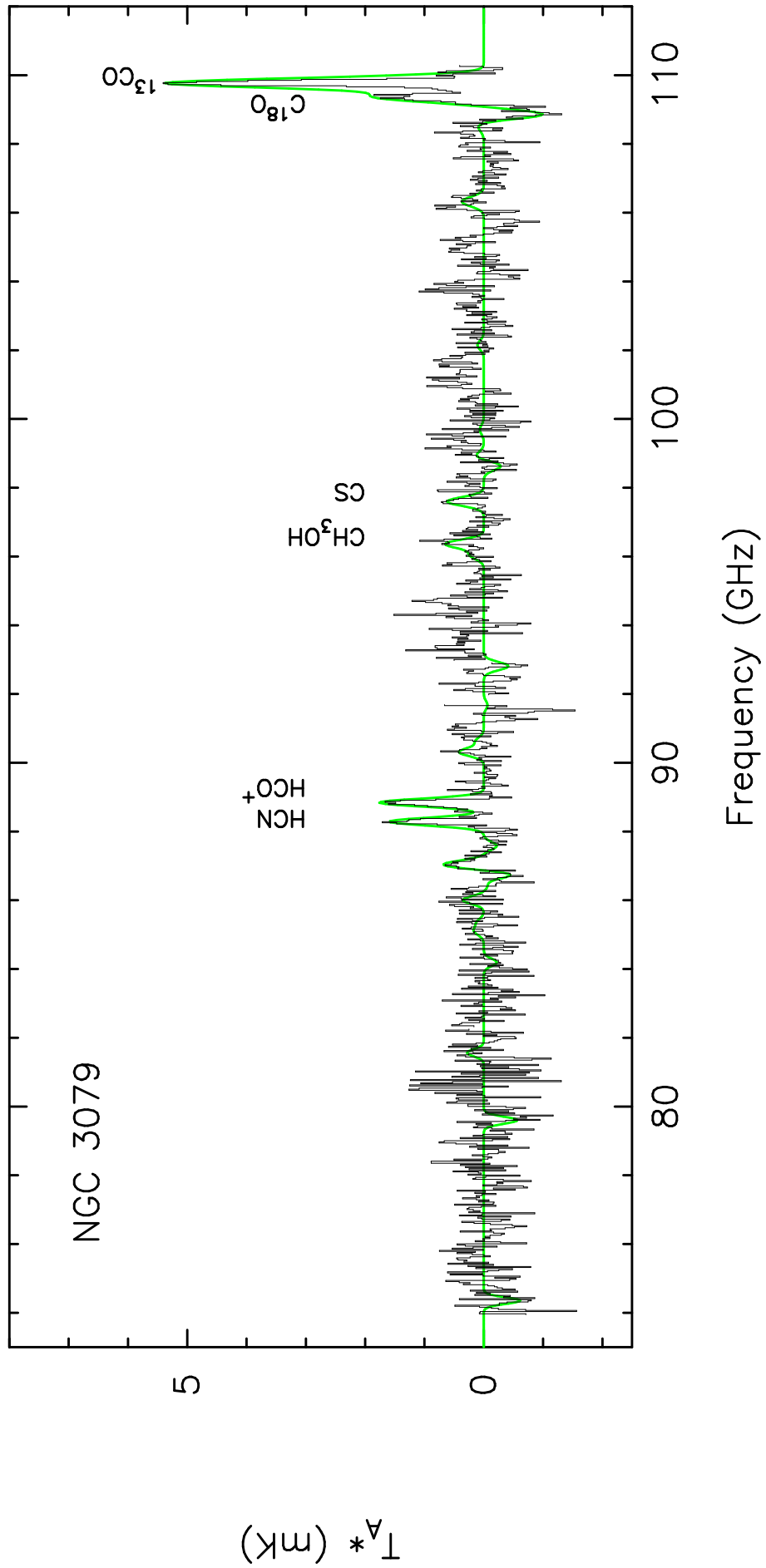


FIG. 1F.— Same as (a) for NGC 3079.

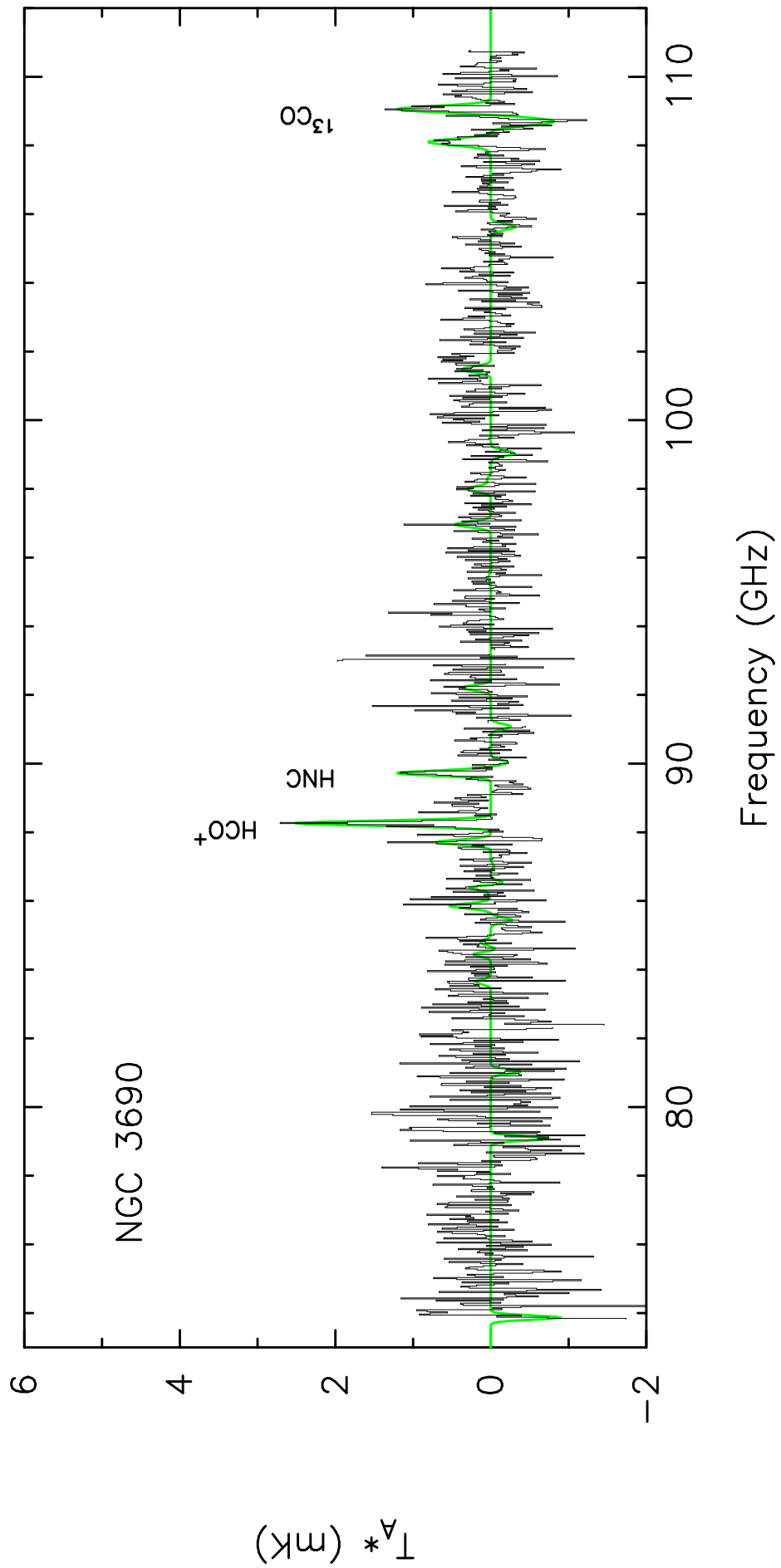


FIG. 1G.— Same as (a) for NGC 3690.

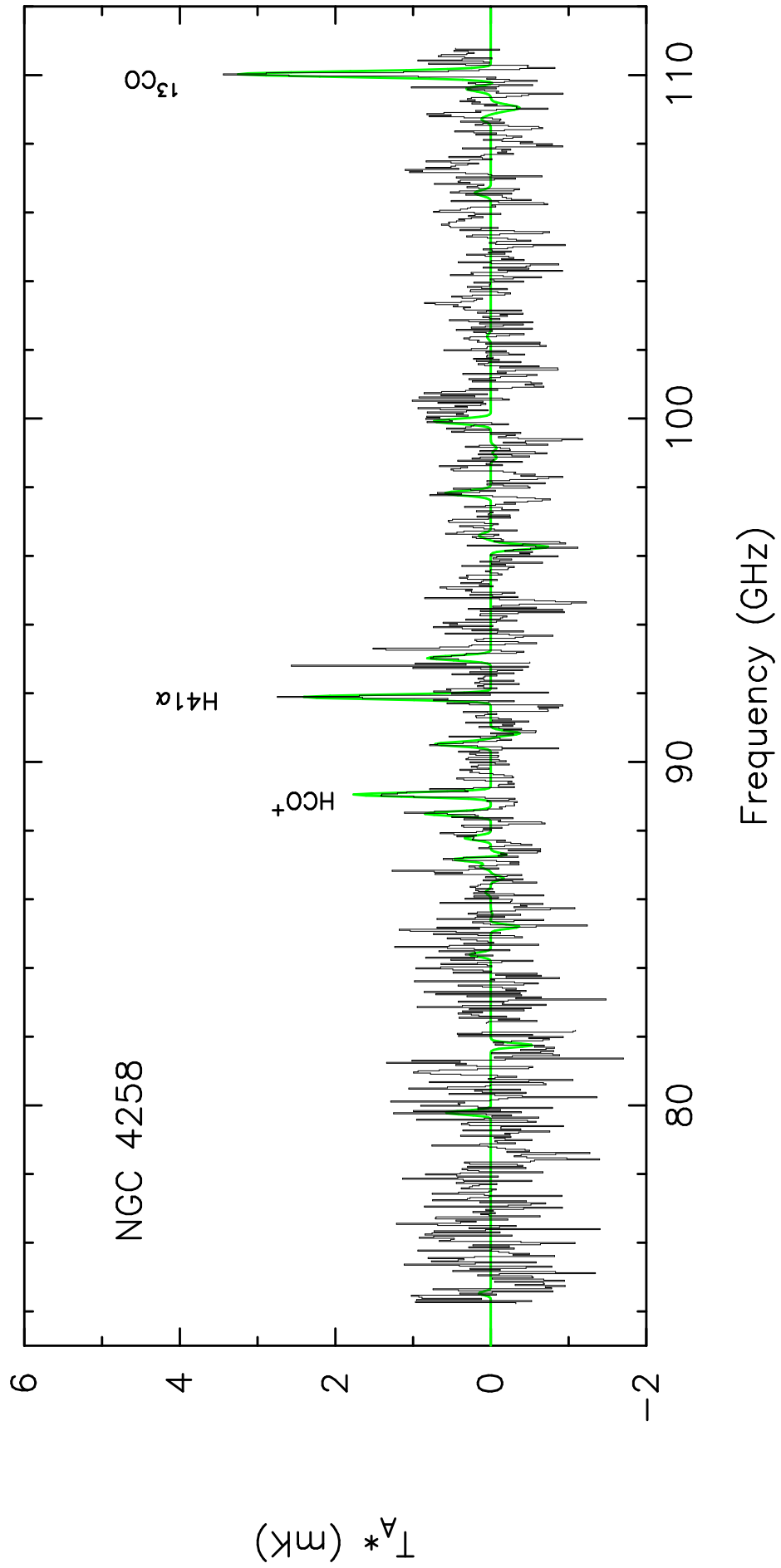


FIG. 1H.— Same as (a) for NGC 4258.

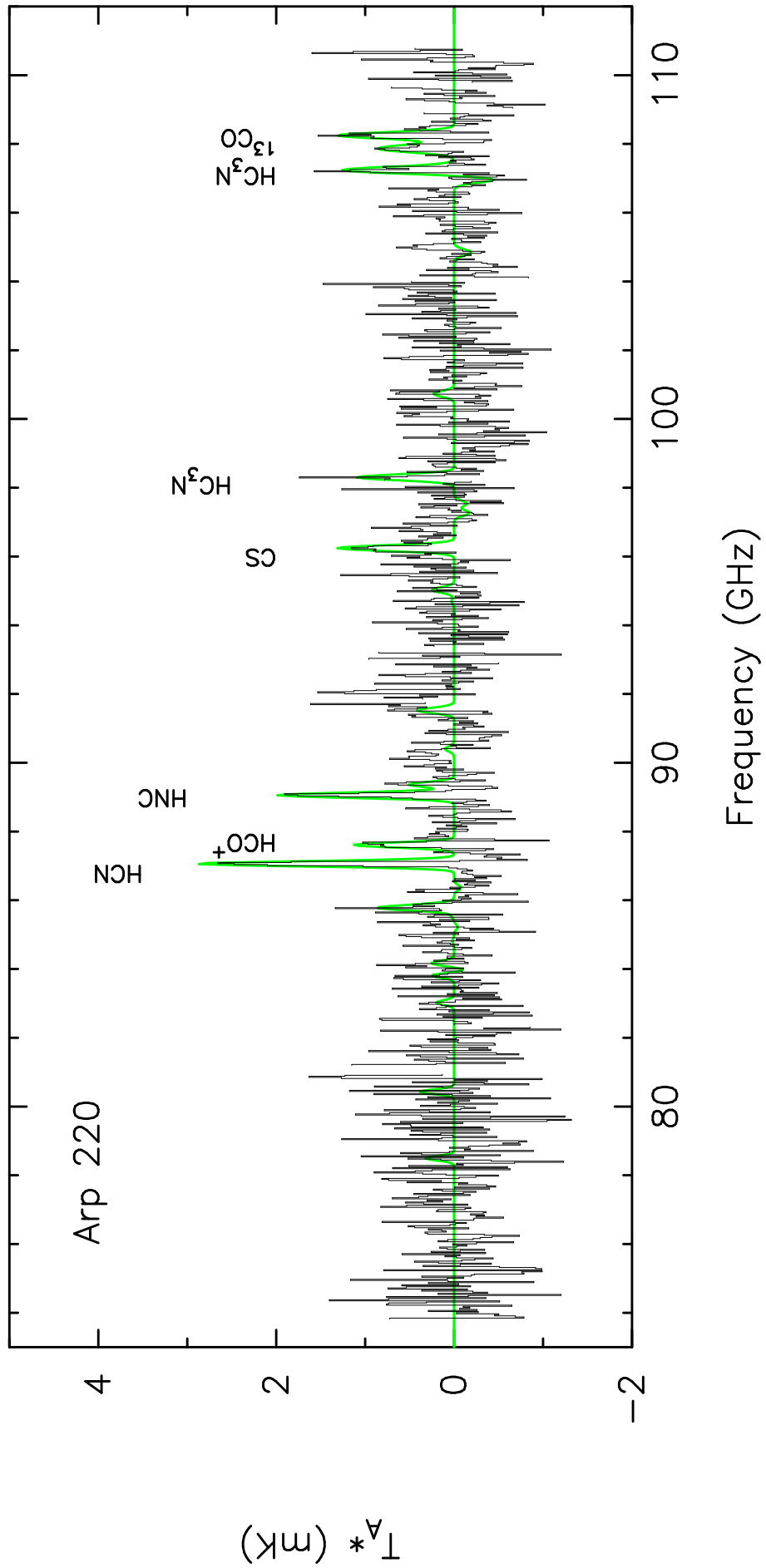


FIG. 11.— Same as (a) for Arp 220.

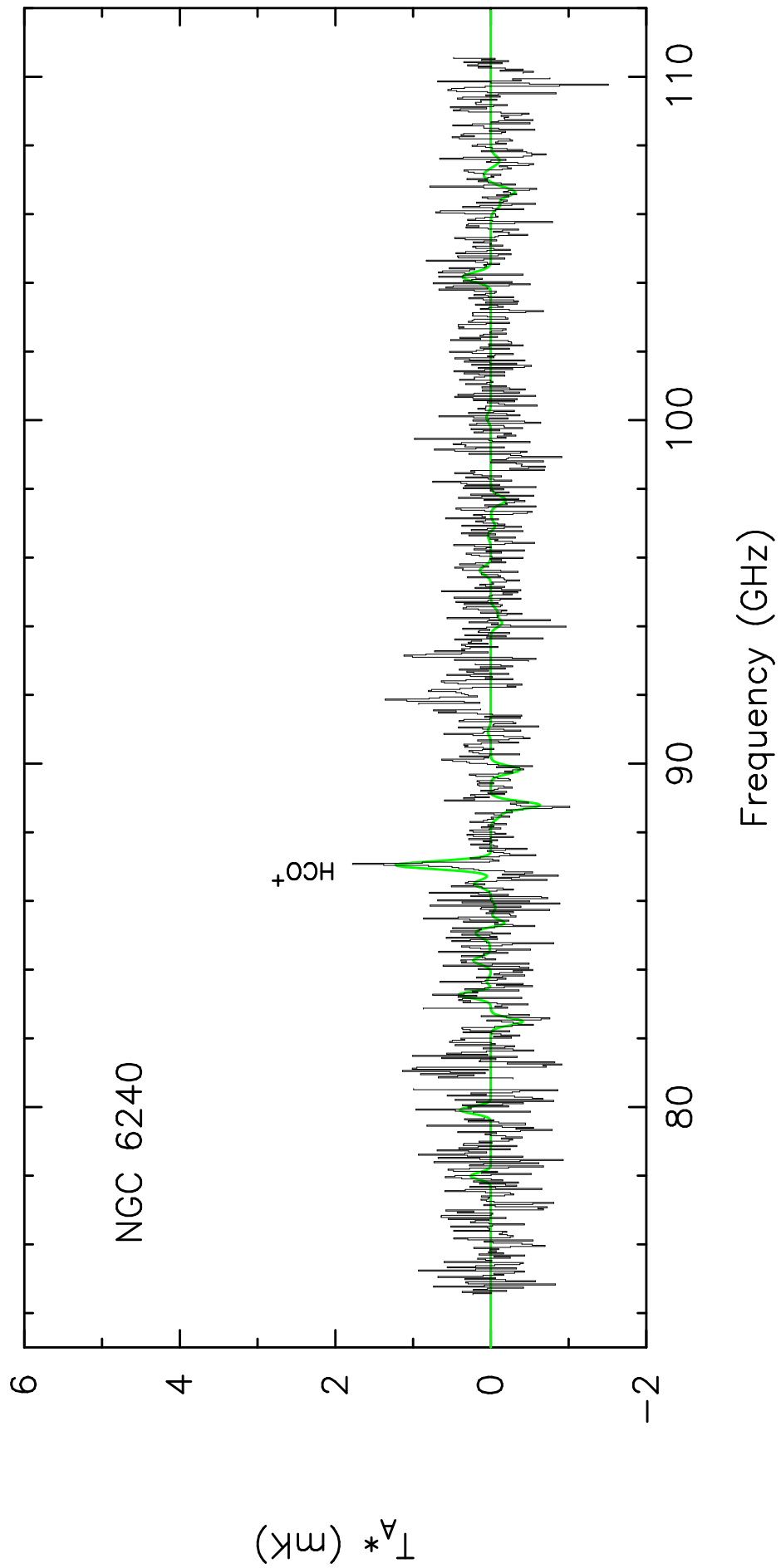


FIG. 1J.— Same as (a) for NGC 6240.

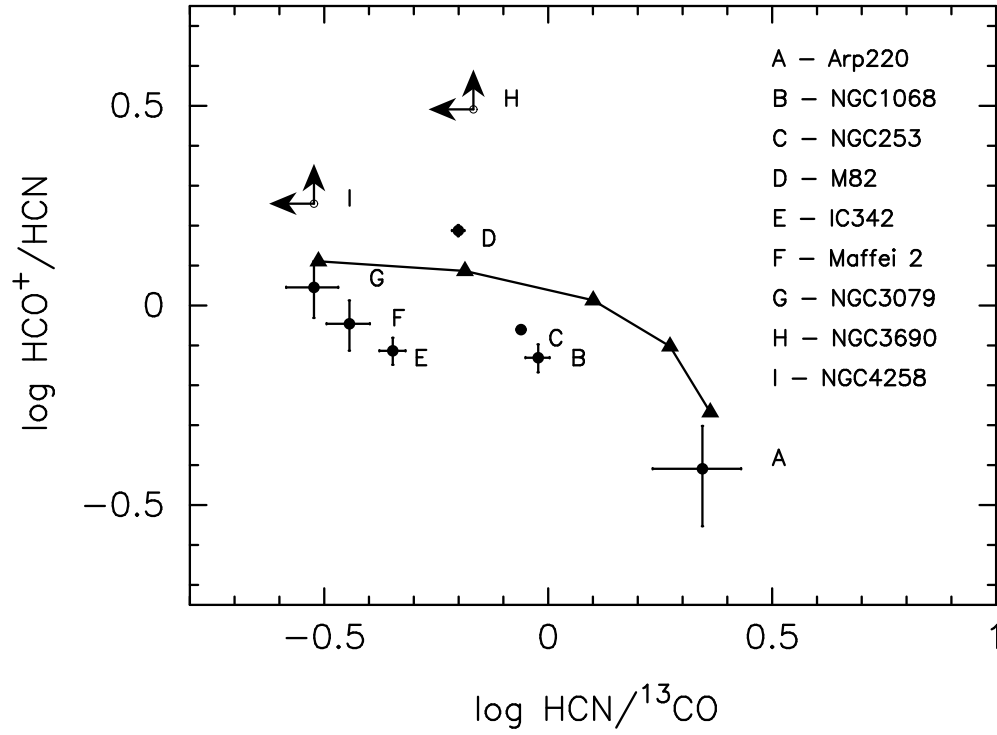


FIG. 2.— A plot of the observed intensity ratio of $\text{HCN}/^{13}\text{CO}$ vs. the observed intensity ratio of HCO^+/HCN for the galaxies (filled circles) where ^{13}CO was detected. The error bars show the 1σ uncertainty in the values of these ratios. In the two galaxies where HCN was not detected, the open circles with arrows mark the 3σ upper limit to the $\text{HCN}/^{13}\text{CO}$ ratio and the 3σ lower limit to the HCO^+/HCN ratio. The results of our modeling of line ratios (see the text in Section 4.1) are shown by the filled triangles with a line connecting five model results with varying density. The models, from left to right, have density of $\log n = 4.0, 4.5, 5.0, 5.5$ and 6.0 .

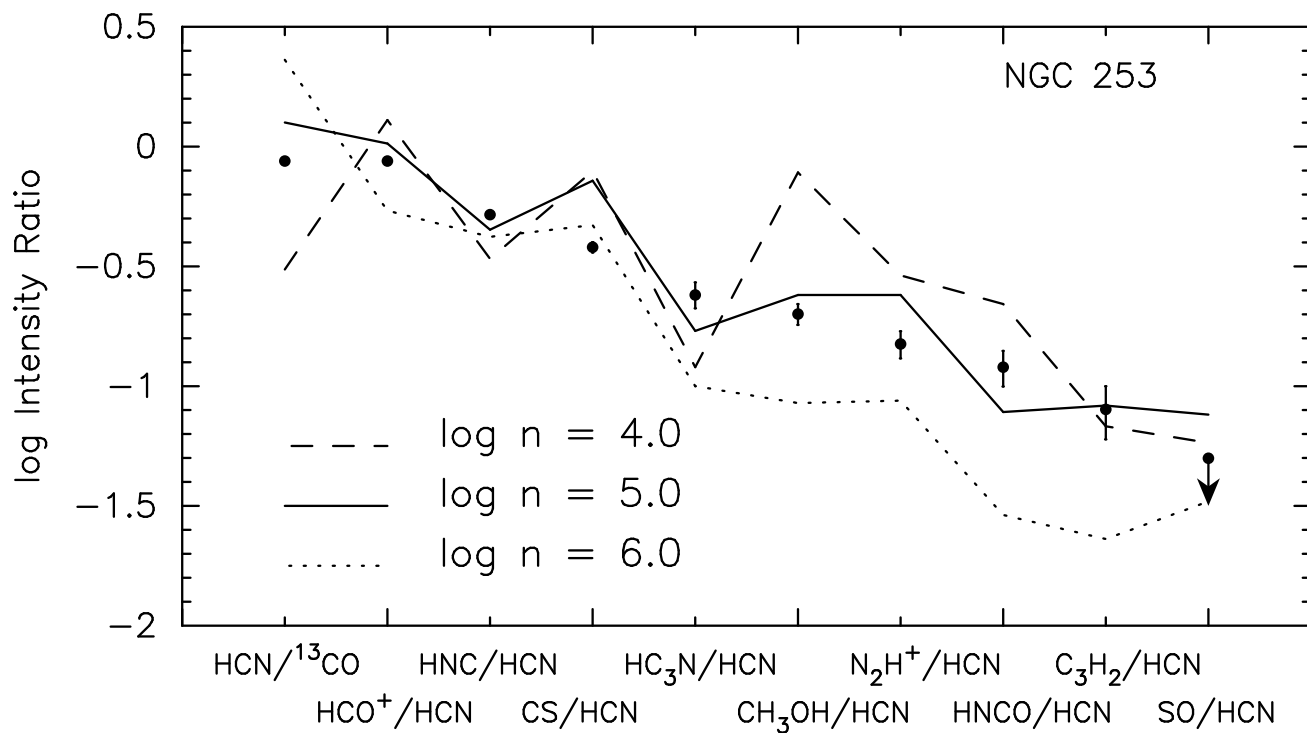


FIG. 3A.— The observed intensity ratios (shown as filled circles) for a number of key molecular species is shown for NGC 253. The error bars show the 1σ uncertainty in the values of the line ratios. Where the molecular species was not detected, the 3σ upper limit on the ratio is shown. Accompanying the observed intensity ratios, are ratios computed from our standard core model, see the text; the modeled line intensity ratios are connected by a dashed line for $\log n = 4.0$, a solid line for $\log n = 5.0$ and a dotted line for $\log n = 6.0$.

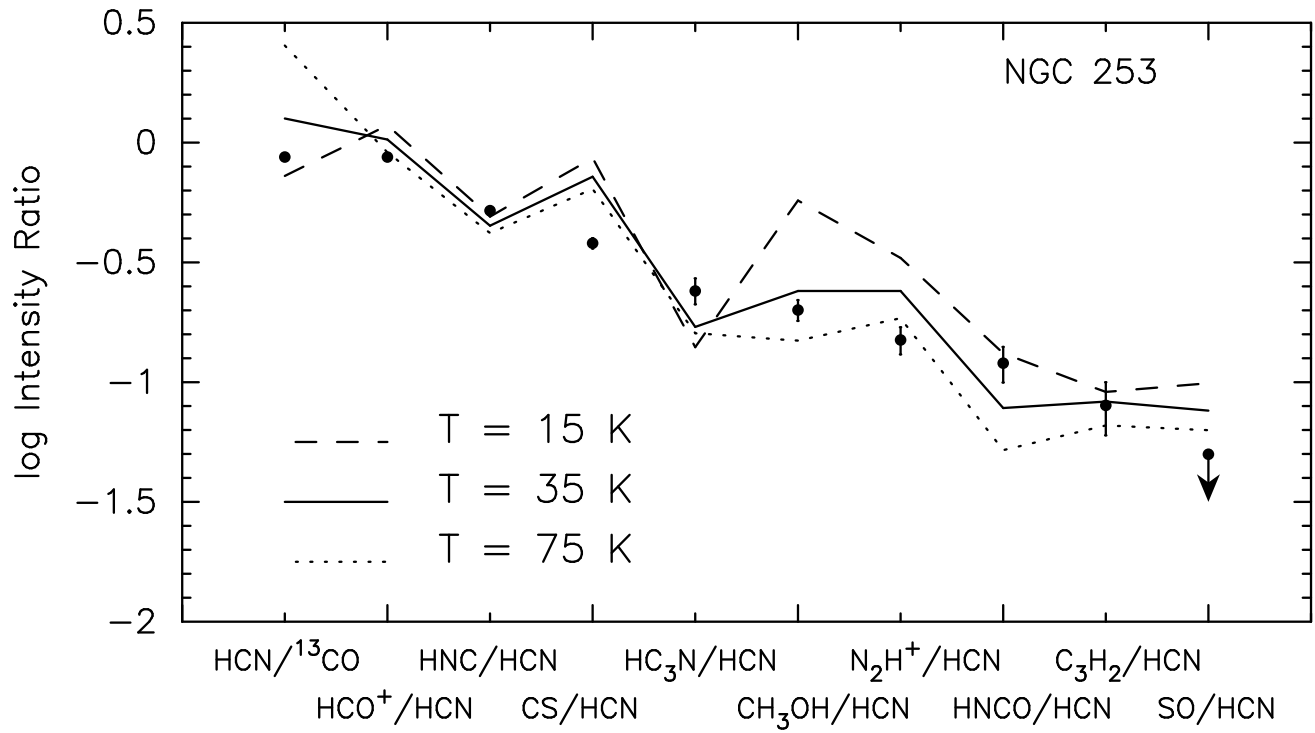


FIG. 3B.— Same as (a), except showing models of the line intensity ratios for fixed density of $\log n = 5.0$, and temperatures of 15 K (dashed line), 35 K (solid line), and 75 K (dotted line).

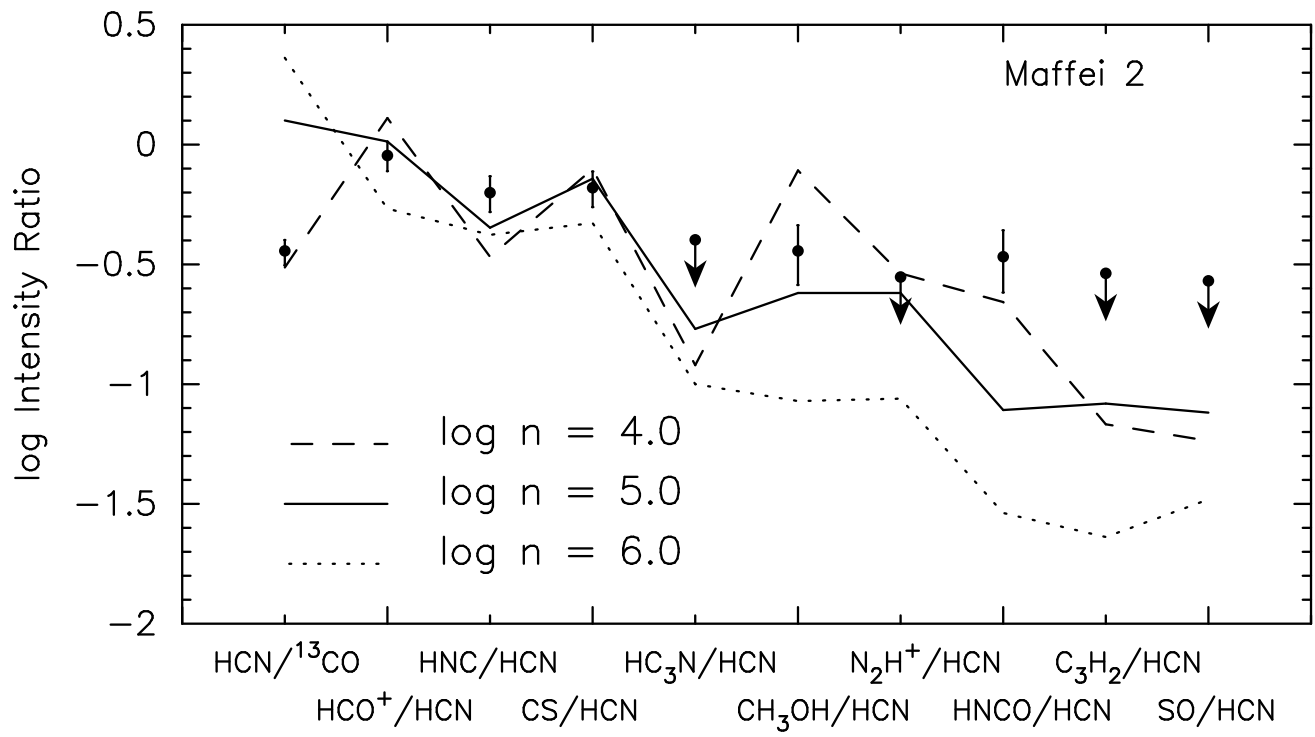


FIG. 4A.— Same as Figure 3(a) for Maffei 2.

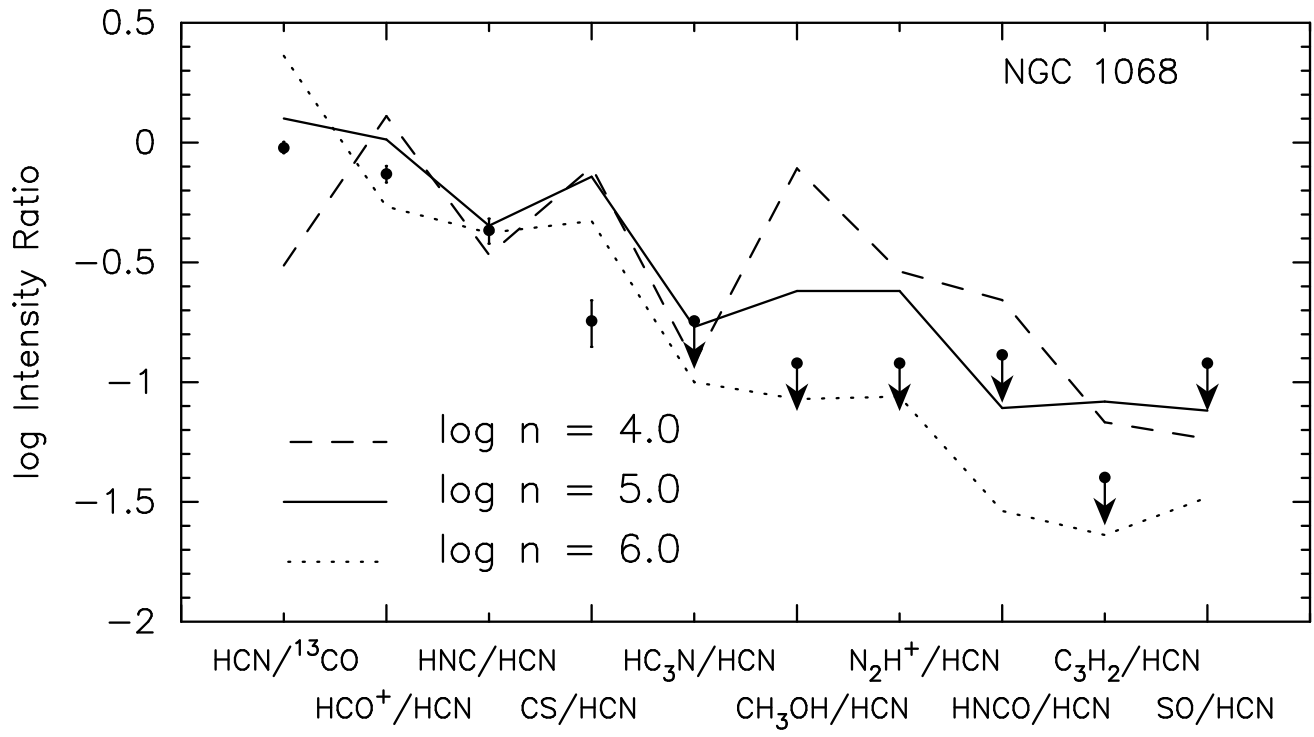


FIG. 4B.— Same as Figure 3(a) for NGC 1068.

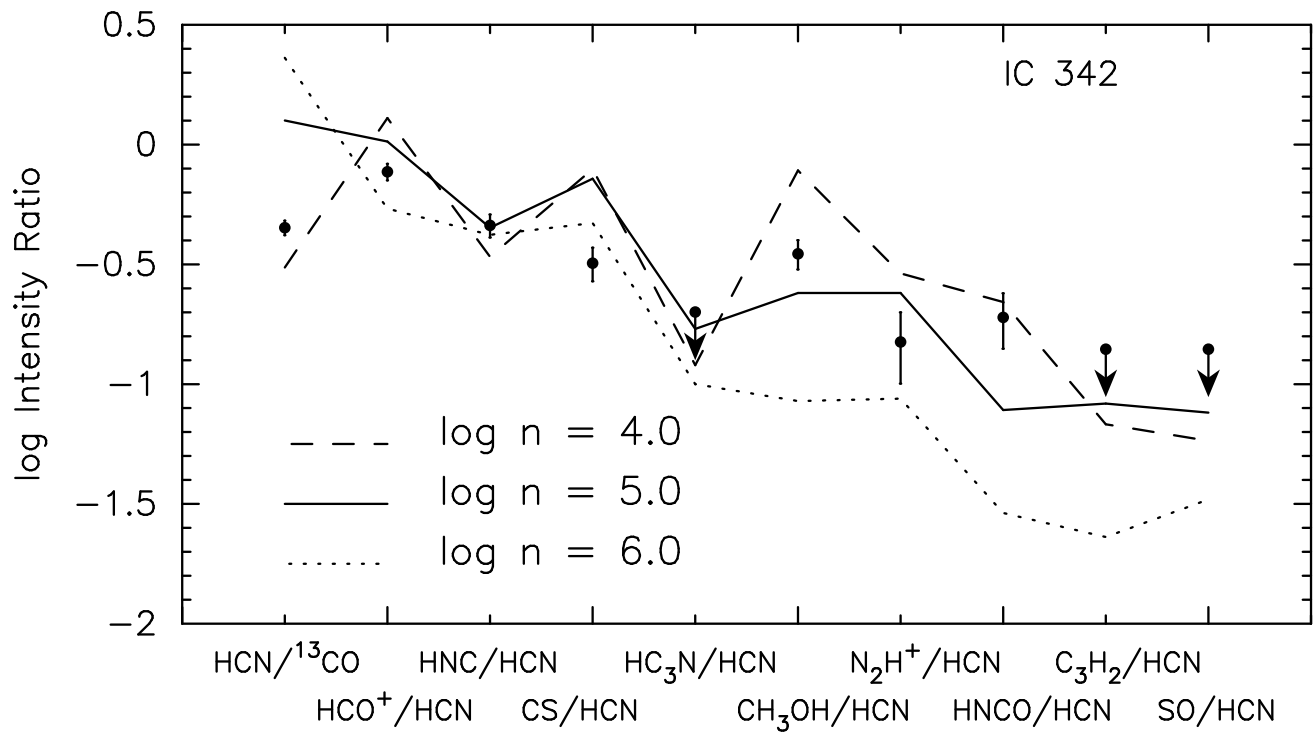


FIG. 4C.— Same as Figure 3(a) for IC 342.

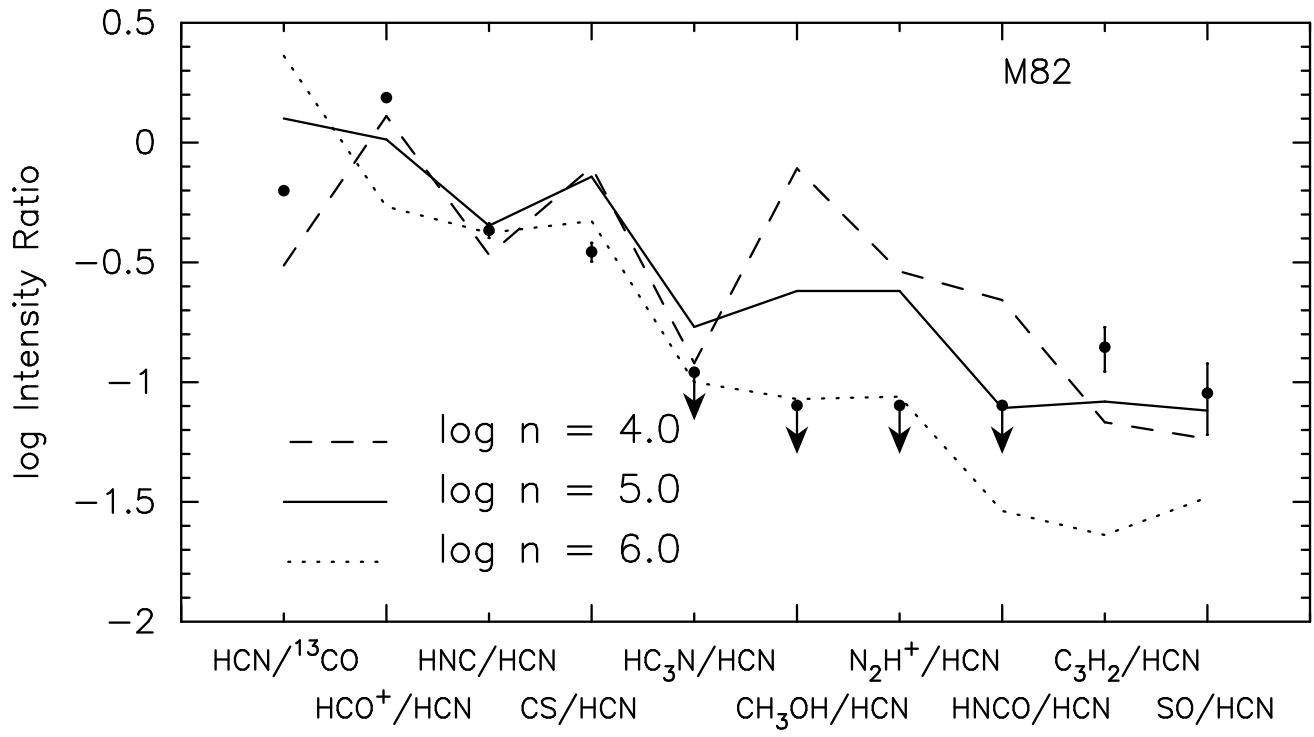


FIG. 4D.— Same as Figure 3(a) for M82.

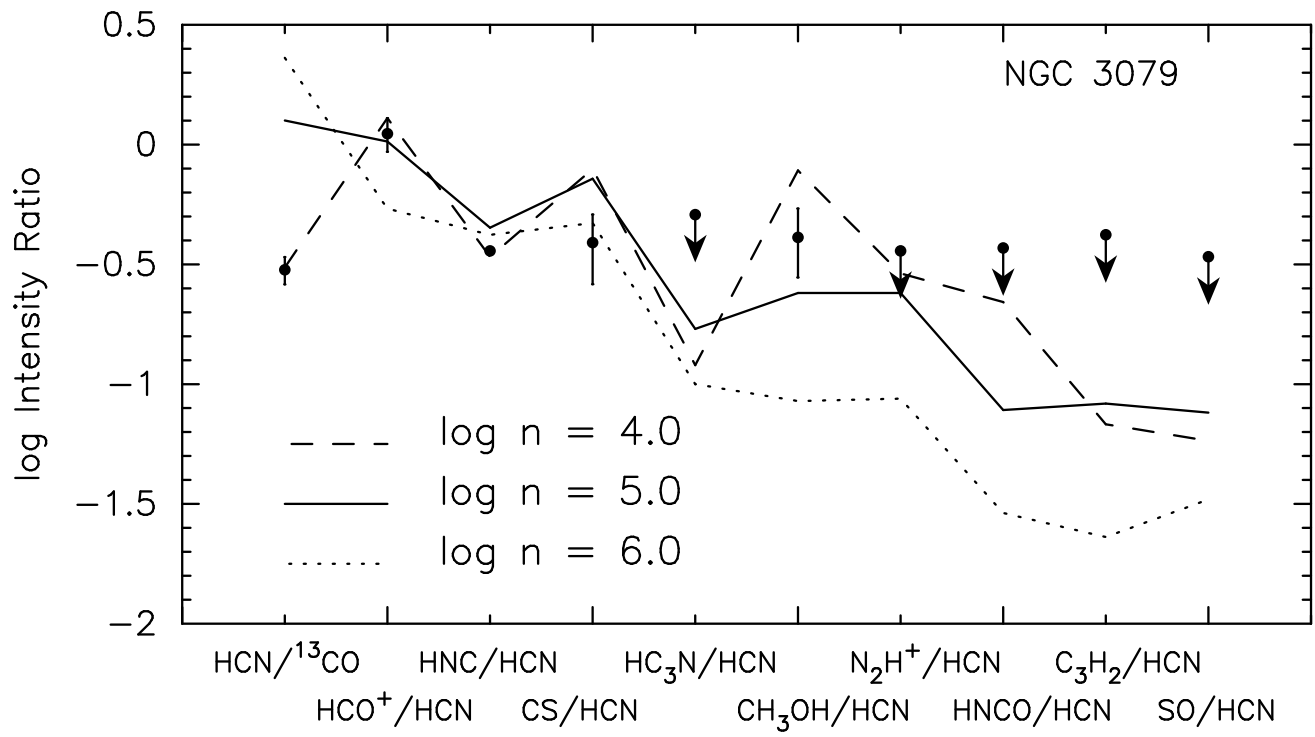


FIG. 4E.— Same as Figure 3(a) for NGC 3079.

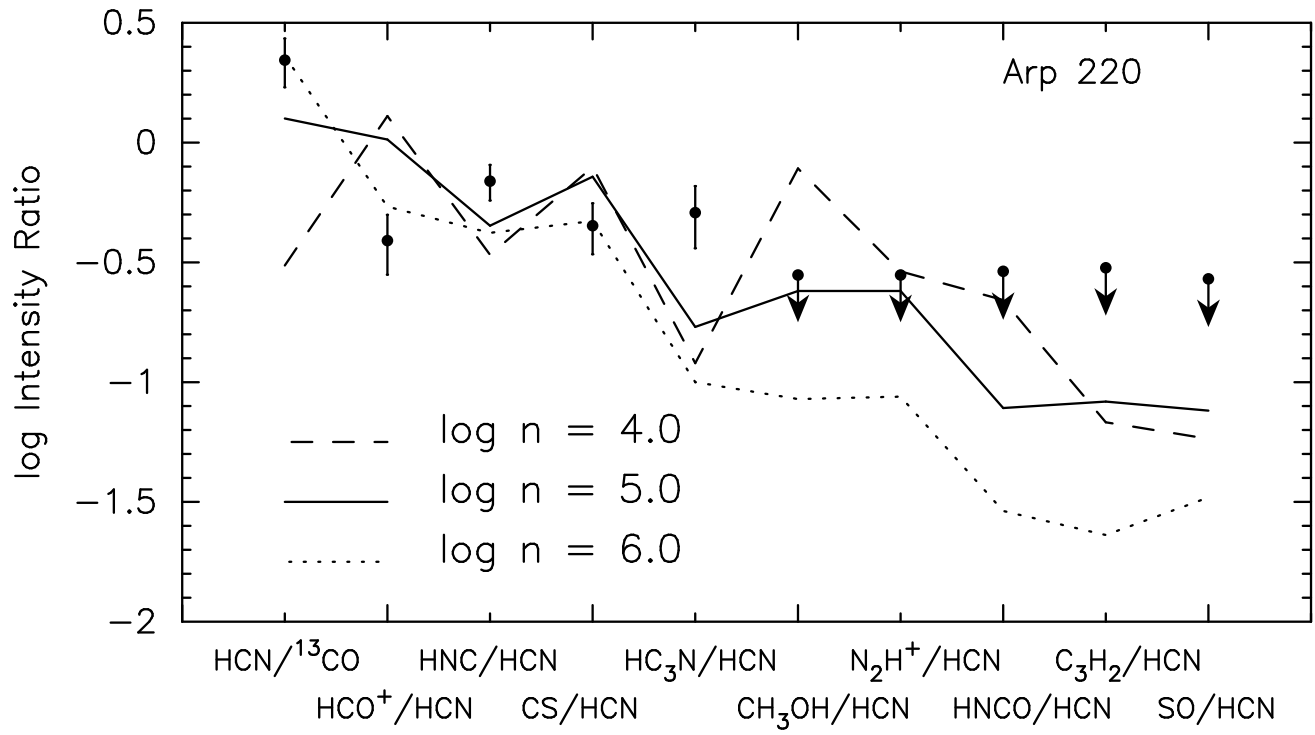


FIG. 4F.— Same as Figure 3(a) for Arp 220.

TABLE 1
GALAXY SAMPLE AND OBSERVING TIMES

Galaxy	$\alpha(2000)^1$	$\delta(2000)^1$	Distance Mpc	t_{int} hr	Notes
NGC 253	00 47 33	-25 17 18	3.9	3.2	Starburst
Maffei 2	02 41 55	+59 36 01	2.8	1.8	Starburst
NGC 1068	02 42 40	-00 00 48	14.4	3.5	Starburst, Seyfert 2
IC 342	03 46 48	+68 05 45	3.3	8.3	Starburst
M82	09 55 52	+69 40 47	3.5	4.3	Starburst
NGC 3079	10 01 57	+55 40 46	19.7	7.5	LINER
NGC 3690	11 28 32	+58 33 43	45	9.0	LIRG, AGN
NGC 4258	12 18 57	+47 18 13	7.9	3.5	Seyfert 2
Arp 220	15 34 57	+23 30 09	76	6.0	ULIRG
NGC 6240	16 52 58	+02 24 03	101	9.7	LIRG, Seyfert 2

¹ Units of right ascension are hours, minutes, and seconds, and units of declination are degrees, arcminutes, and arcseconds.

TABLE 2
FITTED SPECTRAL LINES

Line Number	Frequency (GHz)	Identification
1	74.6446	H44 α
2	79.9127	H43 α
3	81.8815	HC ₃ N 9 - 8
4	84.5211	CH ₃ OH 5(-1) - 4(0) E
5	85.3389	C ₃ H ₂ 2(1,2) - 1(0,1)
6	85.4557	CH ₃ C ₂ H blend
7	85.6884	H42 α
8	86.3402	H ¹³ CN 1 - 0
9	86.7543	H ¹³ CO ⁺ 1 - 0
10	87.0909	HN ¹³ C 1 - 0
11	87.3169	C ₂ H blend
12	87.4020	C ₂ H blend
13	87.9252	HNCO 4(1,3) - 3(1,2)
14	88.6318	HCN 1-0
15	89.1885	HCO ⁺ 1 - 0
16	90.6635	HNC 1-0
17	90.9790	HC ₃ N 10 - 9
18	92.0345	H41 α
19	93.1738	N ₂ H ⁺ 1 - 0
20	96.4129	C ³⁴ S 1 - 0
21	96.7414	CH ₃ OH blend
22	97.9810	CS 1 - 0
23	99.0230	H40 α
24	99.2999	SO 3(2) - 2(1)
25	100.0764	HC ₃ N 11 - 10 (SO 4(5) - 4(4) blended)
26	102.5470	CH ₃ C ₂ H blend
27	106.7374	H39 α
28	108.8939	CH ₃ OH 0(0) - 1(-1) E
29	109.1736	HC ₃ N 12 - 11
30	109.2522	SO 2(3) - 1(2)
31	109.7822	C ¹⁸ O 1 - 0
32	109.9057	HNCO 5(0,5) - 4(0,4)
33	110.2014	¹³ CO 1 - 0

TABLE 3
FITTED LINE INTENSITIES AND LINE WIDTHS

Line Number	Line Intensities ¹									
	NGC253	Maffei 2	NGC1068	IC342	M82	NGC3079	NGC3690	NGC4258	Arp220	NGC6240
1	<2.2	<2.6	<1.5	<1.9	<1.8	<0.6	<0.9	<1.1	<0.9	<0.6
2	<2.1	<2.5	<1.4	<1.7	<1.7	<0.6	<0.9	<1.0	<0.9	<0.6
3	4.7(0.7)	<2.5	<1.4	<1.7	<1.7	<0.6	<0.9	<1.0	<0.9	<0.6
4	<2.0	<2.4	<1.4	<1.7	<1.6	<0.6	<0.8	<1.0	<0.9	<0.6
5	2.9(0.7)	<2.4	<1.4	<1.6	2.7(0.5)	<0.7	<0.8	<1.0	<0.9	<0.6
6	<2.0	<2.4	<1.4	<1.8	<1.6	<0.7	<0.8	<1.0	<0.9	<0.6
7	<2.0	<2.4	<1.4	<1.6	<1.6	<0.6	<0.8	<1.0	<0.9	<0.5
8	<2.0	<2.4	<1.4	<1.6	<1.6	<0.6	<0.8	<1.0	<0.9	<0.5
9	<2.0	<2.4	<1.4	<1.6	<1.6	<0.6	<0.8	<1.0	<0.9	<0.5
10	<2.0	<2.4	<1.4	<1.6	<1.6	<0.6	<0.8	<1.0	<0.9	<0.5
11	9.0(0.7)	<2.4	2.4(0.5)	2.0(0.5)	9.5(0.6)	<0.8	<0.9	<1.0	<0.9	<0.7
12	4.3(0.7)	<2.4	<1.4	<1.6	4.6(0.6)	<0.8	<0.9	<1.0	<0.9	<0.7
13	4.6(0.7)	2.8(0.8)	<1.4	2.2(0.6)	<1.6	<0.6	<0.9	<1.0	<0.8	<0.5
14	37.5(0.7)	8.2(0.8)	10.8(0.5)	11.4(0.6)	20.1(0.6)	1.6(0.2)	<0.8	<1.0	2.9(0.3)	<0.5
15	32.6(0.7)	7.4(0.8)	8.0(0.5)	8.7(0.5)	31.0(0.6)	1.8(0.2)	2.5(0.3)	1.8(0.3)	1.1(0.3)	1.2(0.2)
16	19.4(0.7)	5.2(0.8)	4.7(0.5)	5.2(0.5)	8.6(0.5)	<0.6	1.2(0.3)	<1.0	2.0(0.3)	<0.5
17	3.3(0.7)	<2.3	<1.5	<1.7	<1.6	<0.6	<0.8	<1.0	<0.8	<0.5
18	<2.0	<2.3	1.5(0.5)	<1.5	<1.6	<0.6	<0.8	2.4(0.3)	<0.8	<0.5
19	5.5(0.6)	<2.3	<1.3	1.7(0.5)	<1.6	<0.6	<0.8	<1.0	<0.8	<0.5
20	<1.9	<2.3	<1.3	<1.6	<1.5	<0.6	<0.8	<0.9	<0.9	<0.5
21	7.4(0.6)	3.0(0.8)	<1.3	4.0(0.5)	<1.5	0.6(0.2)	<0.8	<0.9	<0.9	<0.5
22	14.4(0.6)	5.4(0.8)	2.0(0.4)	3.6(0.5)	7.1(0.5)	0.6(0.2)	<0.8	<0.9	1.3(0.3)	<0.5
23	<1.9	<2.2	<1.3	<1.6	<1.5	<0.5	<0.8	<0.9	<0.9	<0.5
24	<1.9	<2.2	<1.3	<1.6	1.8(0.5)	<0.5	<0.8	<0.9	<0.8	<0.5
25	4.4(0.6)	<2.2	<1.3	<1.6	<1.5	<0.5	<0.8	<0.9	1.1(0.3)	<0.5
26	<1.8	<2.2	<1.3	<1.6	2.9(0.5)	<0.5	<0.8	<0.9	<0.8	<0.5
27	<1.8	<2.2	<1.3	<1.5	1.7(0.5)	<0.5	<0.7	<0.9	<0.8	<0.5
28	<1.8	<2.1	<1.2	<1.5	<1.4	<0.6	<0.7	<0.9	<0.8	<0.5
29	<1.9	<2.2	<1.4	<1.5	<1.6	<0.9	<0.9	<1.0	1.2(0.3)	<0.8
30	<1.9	<2.2	<1.4	<1.5	<1.6	<0.9	<0.9	<1.0	<1.0	<0.8
31	9.5(0.6)	2.9(0.7)	2.2(0.4)	6.4(0.5)	7.1(0.5)	1.6(0.2)	<0.8	<0.9	<0.8	<0.6
32	2.7(0.6)	<2.1	<1.2	2.1(0.5)	<1.4	<0.7	<0.8	<0.9	<0.8	<0.6
33	43.2(0.7)	22.7(0.8)	11.4(0.5)	25.6(0.6)	31.8(0.5)	5.3(0.2)	1.2(0.3)	3.3(0.3)	1.3(0.3)	<0.5
Line Width ²	235(3)	202(8)	277(9)	132(4)	253(4)	546(22)	357(37)	305(27)	361(30)	551(75)

¹ Intensities given are the peak T_A^* in mK. The format is intensity with the 1 sigma uncertainty in parentheses. For non-detections, the 3 sigma upper limit on the line intensity is given.

² Line widths are in km s^{-1} . The format is line width with the 1 sigma uncertainty in parentheses.

TABLE 4
ASSUMED MOLECULAR ABUNDANCE RELATIVE TO H_2

Molecular Species	Ratio - GMCs ¹	Ratio - NGC 253 ²
^{13}CO	2×10^{-6}	-
HCN	9×10^{-9}	5.0×10^{-9}
HCO^+	2×10^{-9}	1.6×10^{-9}
HNC	2×10^{-9}	1.0×10^{-9}
CS	6×10^{-9}	6.2×10^{-9}
N_2H^+	3×10^{-10}	-
HC_3N	4×10^{-10}	6.3×10^{-9}
SO	1×10^{-9}	1.3×10^{-9}
CH_3OH	8×10^{-9}	1.3×10^{-9}
C_3H_2	5×10^{-10}	5.0×10^{-10}
HNCO	1×10^{-9}	1.6×10^{-9}

¹ Abundances from Bergin et al. (1997)

² Abundances from Martín et al. (2006)

TABLE 5
 MASS AND BEAM FILLING FRACTION

Galaxy	D_B kpc	f_{area}	Mass from ^{13}CO M_\odot	S_{CO}^1 Jy km s $^{-1}$	Mass from CO M_\odot	Dense Gas Fraction
NGC 253	0.9	0.26	2.7×10^8	1.1×10^4	1.2×10^9	0.23
Maffei 2	0.6	0.11	6.2×10^7	-	-	-
NGC 1068	3.3	0.08	1.1×10^9	2.3×10^3	1.8×10^9	0.61
IC 342	0.8	0.08	6.2×10^7	1.5×10^3	1.2×10^8	0.52
M82	0.8	0.19	1.7×10^8	6.7×10^3	5.8×10^8	0.29
NGC 3079	4.5	0.07	2.0×10^9	1.6×10^3	4.4×10^9	0.45
NGC 3690	10.4	0.01	1.5×10^9	4.5×10^2	6.5×10^9	0.23
NGC 4258	1.8	0.02	1.1×10^8	3.0×10^2	1.3×10^8	0.85
Arp 220	17.5	0.01	4.7×10^9	4.0×10^2	1.6×10^{10}	0.29
NGC 6240	23.2	<0.01	< 4.9×10^9	2.4×10^2	1.7×10^{10}	<0.29

¹ From Young et al. (1995)